



Structural controls and metallogenic model of polyphase uranium mineralization in the Kiggavik area (Nunavut, Canada)

Alexis Grare^{1,2} · Antonio Benedicto³ · Julien Mercadier⁴ · Olivier Lacombe¹ · Anna Trave⁵ · Marie Guilcher⁴ · Antonin Richard⁴ · Patrick Ledru² · Mario Blain² · John Robbins² · Philippe Lach⁶

Received: 5 November 2018 / Accepted: 31 January 2020
© Springer-Verlag GmbH Germany, part of Springer Nature 2020

Abstract

The Kiggavik area is located on the eastern boundary of the Paleo- to Mesoproterozoic Thelon Basin (Nunavut, Canada) and hosts uranium mineralization in Archean basement rocks. The major fault/fracture network in the Kiggavik area is mainly oriented ENE-WSW and NE-SW, consisting of polyphased fault zones initiated during the Thelon and Trans-Hudsonian orogenies (ca. 1900–1800 Ma). These faults were subsequently mineralized in four stages referred to as U0, U1, U2, and U3. The first event U0 is inferred to be of magmatic origin and is related to microbrecciation and weak clay alteration under a WSW-ENE σ_1 . U0 is a ca. 1830 event which predates intense quartz brecciation (QB) and veining at ca. 1750 Ma. QB is associated with emplacement of the Kivalliq Igneous Suite and caused pervasive silicification of former fault zones, which in turn controlled subsequent fracture development and behaved as barriers for later U mineralizing fluids (U1 to U3). U1, U2, and U3 postdate deposition of the Thelon Basin. U1 and U2 occurred under a regional strike-slip stress regime, with the direction of σ_1 evolving from WNW-ESE (U1) to NE-SW /ENE-WSW (U2); both formed at ~1500–1330 Ma and are related to circulation of Thelon-derived uranium-bearing basinal brines. A post U2, but pre-Mackenzie dykes (ca. 1270 Ma), extensional/transensional stress regime with σ_3 oriented NE-SW caused normal-dextral offset of the orebodies by reactivating NNW-SSE and E-W trending faults. This fracturing event triggered circulation of hot (~300 °C), probably acidic, fluids that dissolved quartz, and caused illitization and bleaching of the host rocks. Finally, U3 records remobilization of the previous mineralization along redox fronts through percolation of low-temperature meteoric fluids during two main tectonic events at ca. 550 and 350 Ma. This study provides evidences for the presence of a primary, pre-Thelon Basin uranium stock within the Kiggavik prospects, and a strong structural control on mineralization in the Kiggavik area. Our study also shows a nearly similar evolution of uranium mineralization in this area compared to the world-class uranium district of the Athabasca Basin (Saskatchewan, Canada).

Keywords Uranium · Structural control · Faults and fractures · Kiggavik · Unconformity-related mineralization

Editorial handling: M. Fayek

Electronic supplementary material The online version of this article (<https://doi.org/10.1007/s00126-020-00957-x>) contains supplementary material, which is available to authorized users.

✉ Alexis Grare
alexisgrare@gmail.com

¹ Sorbonne Université, CNRS-INSU, Institut des Sciences de la Terre de Paris, Paris, France

² Orano Canada Inc., 817-45th St West, Saskatoon, SK S7L 5X2, Canada

³ Université Paris Sud, UMR GEOPS, 91405 Orsay, France

⁴ CNRS, CREGU, GeoRessources lab, Campus Aiguillettes, Faculté des Sciences et Technologies, Université de Lorraine, rue Jacques Callot, 54506 Vandoeuvre-lès-Nancy, France

⁵ Departament de Mineralogia, Petrologia i Geologia Aplicada, Facultat de Ciències de la Terra, Universitat de Barcelona, 08028 Barcelona, Spain

⁶ BRGM French Geological Survey, 3 avenue Claude Guillemin, BP 36009, 45060 Orléans Cedex 2, France

Introduction

Numerous uranium occurrences have been discovered since the 1970s in the Thelon-Baker Lake area of Nunavut, Canada (Curtis and Miller 1980; Miller 1980, 1982, 1995; Miller and LeCheminant 1985; Miller et al. 1986). In this area, the Paleoproterozoic Thelon Basin is similar in terms of sedimentology, geology, structural evolution, and diagenetic history with the Athabasca Basin (Saskatchewan, Canada) that is located approximately 750 km south-west and hosts the largest number of high-grade unconformity-related uranium (URU) deposits in the world (Miller and LeCheminant 1985; Fuchs et al. 1986; Weyer et al. 1987; Friedrich et al. 1989; Fuchs and Hilger 1989; Jefferson et al. 2007). Among the prospective zones, the Kiggavik area, located on the eastern border of the Thelon's Aberdeen sub-basin (Fig. 1), hosts several U orebodies of economic interest: Kiggavik (Main Zone, Center Zone, East Zone), Bong, Andrew Lake, and End prospects, in addition to the Granite grid, 85W, Sleek, Jane and Contact minor prospects (Fig. 2; Fuchs et al. 1986; Riegler et al. 2014; Chi et al. 2017; Roy et al. 2017).

Various scientific studies have been carried out on these orebodies in order to characterize the key parameters which controlled the formation of U mineralization, with the objective of comparing them with those of the world-class URU deposits in the Athabasca Basin (Jefferson et al. 2007; Cuney and Kyser 2009). Previous studies in the Kiggavik area mainly focused on the characterization of mineralizing fluids and their alteration products through analysis of fluid inclusions, geochemistry, and dating of U oxides and related clay minerals (Farkas 1984; Riegler et al. 2014; Sharpe et al., 2015; Chi et al. 2017; Shabaga et al. 2017). The tectonic history, the related structural controls, and the relative timing of U mineralization in the prospects have not been studied in detail, and are consequently poorly understood, despite being key parameters for the URU mineralization. A study of the Contact prospect (Grare et al. 2017, 2018a) has provided a detailed picture of the successive pre- and syn/post-Thelon fracturing/faulting events at different scales and their role in the formation of U mineralization. A major difference with the Athabasca Basin, where ductile to brittle tectonics involving reactivated Hudsonian graphitic-rich shear zones exerted a major structural and metallogenic control on the formation of the U mineralization (Martz et al. 2017; Pascal et al. 2015), is that the tectonic style of deformation in the Kiggavik area is dominantly brittle, as exemplified by prevailing cataclastic to ultracataclastic fault rocks (Grare et al. 2018a, b). Graphite is also almost absent from the basement lithologies and faults within the Kiggavik area.

Based on the study of fluid inclusions in quartz-carbonate veins spatially associated with U mineralization at the End prospect, Chi et al. (2017) proposed that U mineralization initially formed from high salinity (> 25 wt% eq NaCl +

CaCl₂), 80–200 °C Na- to Ca-rich basinal brines derived from the Thelon Basin. These Na- to Ca-rich basinal brines are slightly more saline than the original Na-dominated diagenetic fluids defined within the Thelon Basin (Renac et al. 2002) but are similar in terms of temperature and composition to the mineralizing fluids in the URU deposits of the Athabasca Basin (Pagel 1975; Kotzer and Kyser, 1995; Derome et al. 2005; Richard et al. 2010, 2012, 2016; Chu and Chi 2016; Martz et al. 2018; Wang et al. 2018). For the Bong prospect, Sharpe et al. (2015) proposed a five-stage metallogenic model with primary U mineralization occurring at ca. 1500 Ma, followed by different U mineralization stages/remobilization almost until the present time. The nature of the mineralizing fluids are unconstrained for the first stage and those related to the second stage of mineralization (at 1100 Ma) are isotopically closer to meteoric water than to basinal brines. On the basis of chemical characterization and dating of alteration and U mineralization, Shabaga et al. (2017) proposed that three mineralization events (ca. 1030 Ma, 530 Ma and < 1 Ma) formed the Andrew Lake deposit and that fluids were initially dominantly meteoric and oxidizing and secondly became more acidic. Illite-chlorite-U oxide association is commonly observed (Riegler et al. 2014; Sharpe et al., 2015; Chi et al. 2017; Shabaga et al. 2017) for the primary stage of mineralization in the whole Kiggavik area. The hydrothermal chlorite is dominantly sudoitic in composition, as observed for the hydrothermal chlorite linked to U mineralization in the Athabasca Basin (Hoeve and Quirt 1984; Kotzer and Kyser 1995).

Anand and Jefferson (2017) display a structural synthesis for the Kiggavik area established from satellite imagery, geophysical interpretations, and field observations in which a district-scale structural evolution from ca. 2760 to 447 Ma is proposed, encompassing multiple reactivations of a Riedel shear system. Their approach contrasts with the detailed sequence of fracturing/faulting events published by Grare et al. (2018a) for the Contact prospect that was reconstructed on the basis of both macroscopic (drill core and field data) and microscopic (optical microscopy, cathodoluminescence and SEM) paragenetic observations, and which includes precise chronological constraints.

This review of previous works highlights that the nature of the U mineralization at Kiggavik and its controls (structural, fluid, timing, and physico-chemical) are still under debate. Despite the work by Anand and Jefferson (2017) that provides insights into the succession of regional tectonic events, the link between the macroscale and the microscale fractures and U mineralization, and the 3D architecture of faults zones in the Kiggavik area remains unconstrained. These points need however to be carefully addressed in order to build a complete metallogenic model of U mineralization in the Kiggavik area.

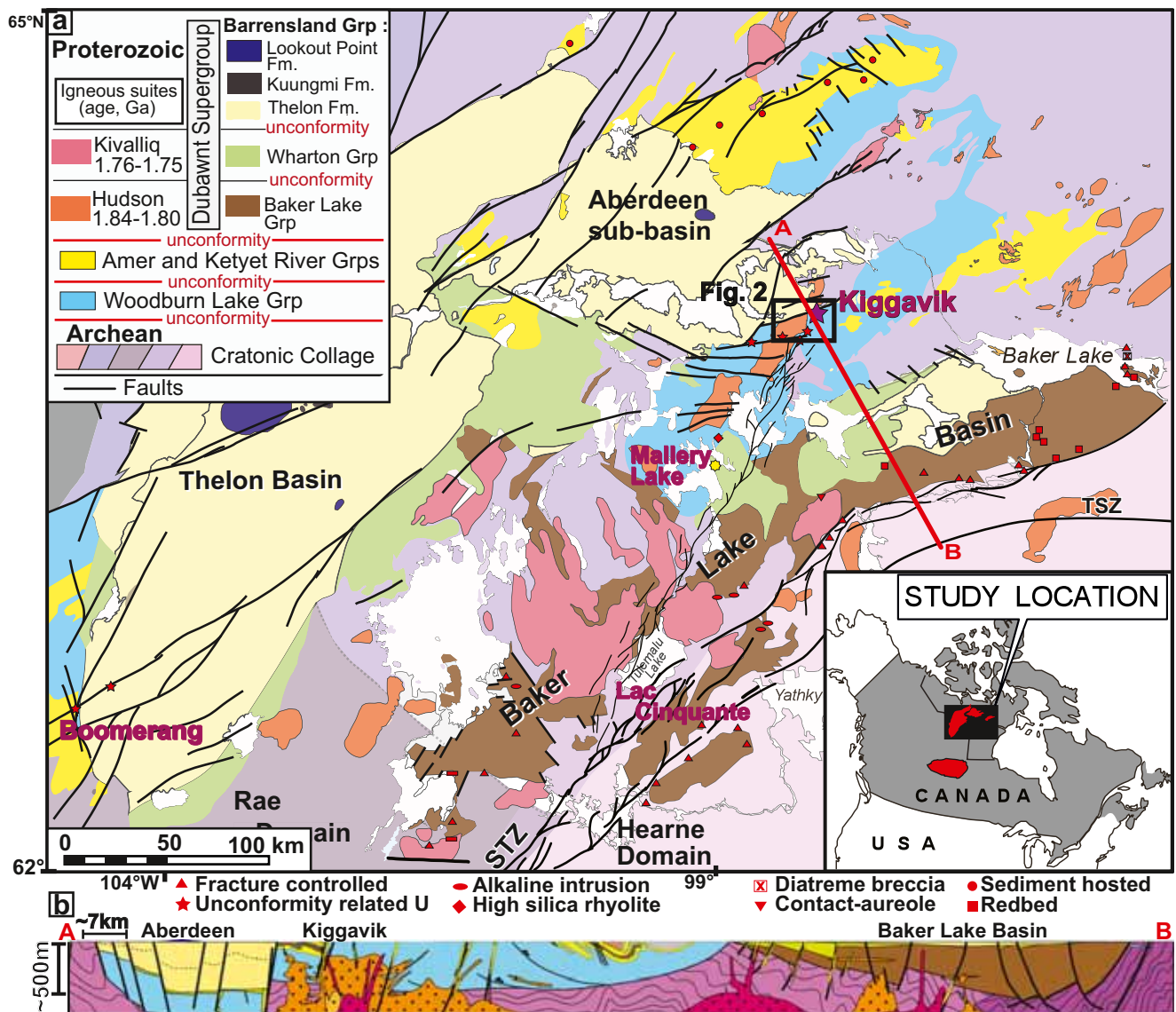


Fig. 1 a Geological map of the Thelon-Baker Lake area (after Curtis and Miller 1980; Rainbird et al. 2003). b Geological cross-section from the Aberdeen sub-basin to Baker Lake basin, modified after Jefferson et al. 2011; Hadlari and Rainbird 2011; Pehrsson et al. 2013)

The twofold aim of this contribution is (1) to depict the brittle tectonic stages and the spatial-temporal structural evolution that led to the formation of the fault/fracture network that controls U mineralization in the Kiggavik area, and (2) to constrain the nature of the paleo-fluids and the conditions and timing of their circulation through the identified fracture networks by the analysis of the resulting fluid-rock interactions (cements, clays, ore minerals), and U mineralization. As an outcome of this multi-source approach, we propose an integrated structural and metallogenic model for the formation of the U mineralization in the Kiggavik area and make comparisons with the world-class URU mineralization from the Athabasca Basin. This model includes both pre-Thelon and post-Thelon Basin U ore formation stages, and for the first time fully illustrates the genesis and evolution of U

mineralization of the prospective Kiggavik area and related Thelon Basin.

Geological setting

Regional setting

The Thelon Basin and the Athabasca Basin are Proterozoic intracratonic basins (Gall et al. 1992; Creaser and Stasiuk, 2007; Davis et al. 2011; Hiatt et al. 2003; Jeanneret et al. 2017) hosted in the Churchill Province. The Churchill Province resulted from the collisional amalgamation of the Rae and Hearne cratons along the Snowbird Tectonic Zone (STZ), either in the Neoproterozoic or during the Snowbird

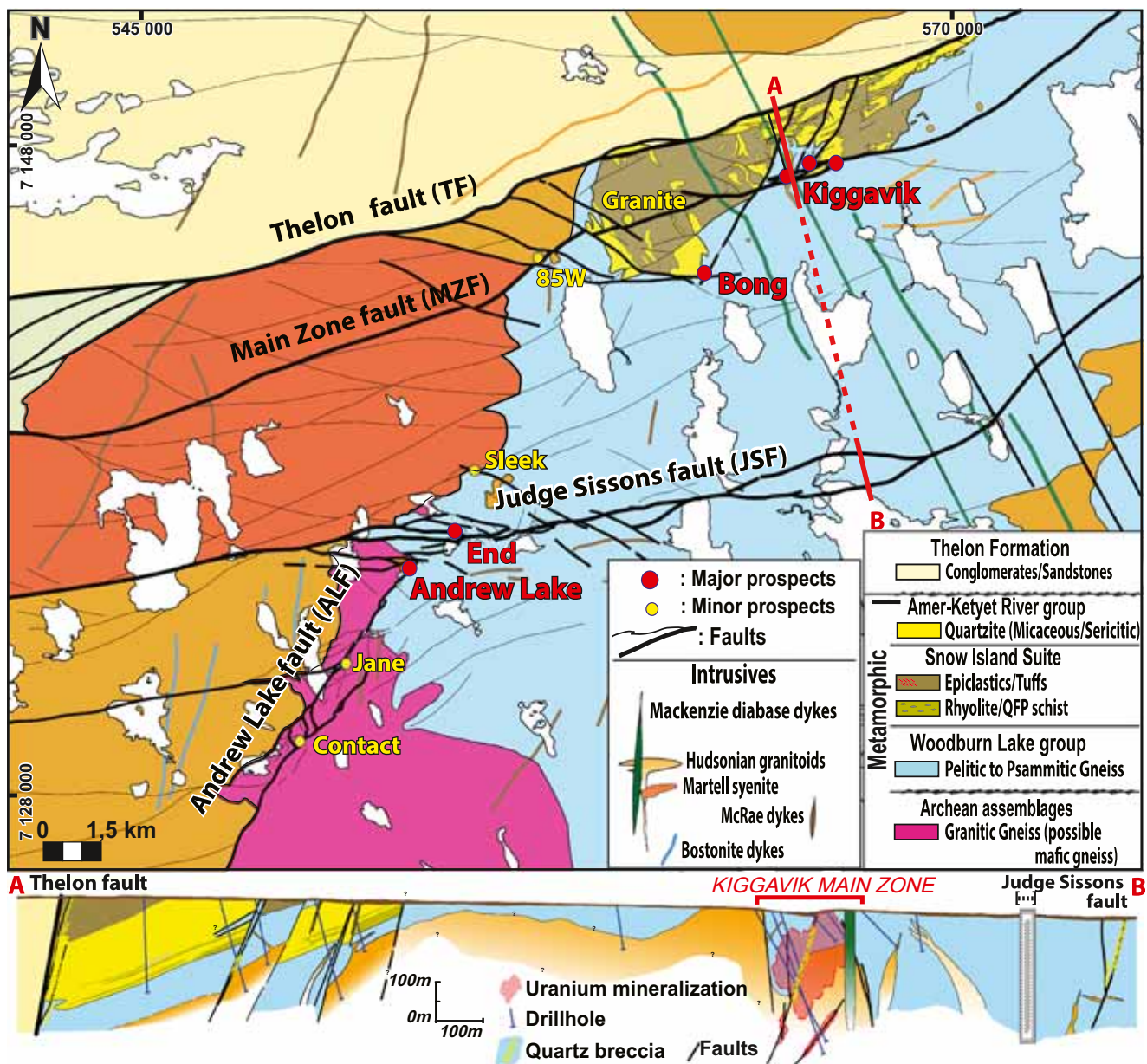


Fig. 2 Simplified geological map of the Kiggavik area (Orano internal document) and cross-section from the Thelon fault to the Judge Sissons fault

orogenesis at ~1.9 Ga (Hoffman 1988; Corrigan et al. 2009; Fig. 1). These basins are located between the eroded remnants of the Trans-Hudson orogenic belt to the southeast (ca. 2070–1800 Ma, overall NW-SE shortening) and the Thelon-Taltson orogenic belt to the west (ca. 2020–1900 Ma, overall E-W shortening). The Thelon Basin mainly consists of the Thelon Formation, a 1800-m-thick sedimentary pile of conglomerates and coarse-grained sandstones, overlain by the ca. 1540 Ma shoshonitic basalts of the Kuungmi Formation (Chamberlain et al. 2010) and marine dolomites from the Lookout Point Formation (Gall et al. 1992) of the Barrenland Group (Fig. 1).

The Thelon Formation unconformably overlies a complex set of sedimentary and bimodal volcanic-sedimentary rocks that infilled the Baker Lake Basin between 1850 and

1750 Ma (Rainbird et al. 2006; Rainbird and Davis 2007). The Baker Lake Basin formed as a result of retro-arc extensional to transtensional rifting tectonics related to the collision between the Churchill province and the Superior province (i.e., the Trans-Hudsonian orogeny). It was followed by uplifting, extensive erosional peneplanation, and regolith formation, then by deposition of the Thelon Formation in response to thermal subsidence (Rainbird et al. 2003; Rainbird and Davis 2007; Hadlari and Rainbird 2011). The Barrenland, Wharton, and Baker Lake groups are parts of the Dubawnt Supergroup (Peterson, 2006) (Fig. 1) which overlies the metamorphosed Archean basement. The latter comprises ca. 2870-Ma granitic gneisses (Davis et al. 2006), 2730–2680-Ma supracrustal rocks of the Woodburn Lake

Group (Pehrsson et al. 2013), and a distinctive package of 2620–2580-Ma felsic volcanic and related hypabyssal rocks known as the Snow Island Suite (Jefferson et al. 2011; Peterson 2015; Johnstone et al. 2016). These groups are overlain by the Paleoproterozoic (2300–2150 Ma, Rainbird et al. 2010) orthoquartzite of the Ketyet River Group (Fig. 2). These lithologies, especially the Woodburn Lake Group, host the U mineralization in the Kiggavik area (Fig. 2).

The Archean to Paleoproterozoic rocks of the Churchill province were intruded by three intrusive suites: (i) the late syn-orogenic (ca. 1830 Ma) Hudson suite (Peterson et al. 2002); (ii) the Dubawnt minette suite, contemporaneous of the Hudson suite, with ultrapotassic rocks, minette dykes, and lamprophyres; and (iii) the rapakivi-style Nueltin granite of the anorogenic (ca. 1750 Ma) Kivalliq igneous suite (Hoffman 1988; van Breemen et al., 2005; Peterson et al. 2015; Scott et al. 2015). Minor U mineralization is hosted in fractures and faults developed in Hudson granitoids at the 85W prospect. Dykes of the Mackenzie diabase swarm (1267 ± 2 Ma; LeCheminant and Heaman 1989) form prominent linear aeromagnetic features trending NNW-SSE (Tschirhart et al. 2013, 2017). They cut across all of the previous lithologies and represent the last magmatic-tectonic event in the region.

Local setting, main fault structures, and tectonic evolution

In the Kiggavik area, the basement lithologies are intruded by the Schultz Lake Intrusive Complex (SLIC) (Scott et al. 2015). The SLIC are comprised from two intrusive suites as described by Scott et al. (2015): (i) the “Hudson granite,” non-foliated granitoid sills, syenite, and lamprophyre dykes of the late syn-orogenic Hudson suite; and (ii) the “Nueltin granite,” anorogenic granite to rhyolite of the Kivalliq Igneous Suite (KIS; Peterson et al. 2015). Uranium and thorium primary enrichment were described to be associated with bostonite dykes (Peterson et al. 2011) and pegmatites attributed to emplacement of the Dubawnt minette (ca. 1830 Ma) and KIS, respectively. Such bostonite dykes were observed near the Kiggavik Main Zone (Anand and Jefferson 2017). These rocks are unconformably overlain by the Thelon Formation, which crops out in the northern part of the Kiggavik property (Fig. 2). Several dykes of the Mackenzie swarm form NNW-SSE lineaments and are also observed in the area.

The main structural features in the Kiggavik area are the ENE-trending Thelon Fault, the ENE-trending Main Zone fault in the northern part of the property, the ENE-trending Judge Sissons Fault in the central part, and the NE-trending Andrew Lake Fault in the southwestern part (Fig. 2). The Main Zone fault hosts the 85W, Granite grid, and Kiggavik (main, central, and east zones) occurrences. The End prospect is hosted by the Judge Sissons Fault, while Andrew Lake,

Jane, and Contact occurrences lie along the Andrew Lake Fault (Fig. 2).

Little is known of the long tectonic history predating the Trans-Hudsonian orogeny; however, it is probable that the tectonic initiation of the main faults in the Kiggavik area dates back to the convergence of cratonic blocks during the latest stage of Trans-Hudsonian orogeny. The Thelon Fault constitutes the contact between the siliciclastic sedimentary rocks of the Thelon Formation to the north and the metamorphosed basement rocks to the south (Fig. 2). South of the Thelon Fault, magnetic maps show that the SLIC is cross-cut by numerous ENE-trending parallel and sub-parallel faults with apparent right-lateral displacement (Tschirhart et al. 2017). The steep northward dip of the Judge Sissons Fault was inferred from observations in discontinuous outcrops and on drill cores. The Andrew Lake Fault constitutes the mapped boundary between the Hudson granite to the west and the metamorphosed basement rocks to the east (Fig. 2). The Andrew Lake Fault is delineated from interpretation of aeromagnetic and ground gravity maps (Fig. 2) (Roy et al. 2017; Tschirhart et al. 2017), as outcrops are nearly absent.

The study of the Contact prospect (Grare et al. 2018a) provided new insights into the structural evolution of the Andrew Lake Fault, which also included a post-Thelon U mineralization event. Grare et al. (2018a) highlighted the presence of an extensive silicification event along the Andrew Lake Fault, characterized by a quartz-healed breccia, termed the Quartz Breccia (QB, Grare et al. 2018b). This structure is a main feature of both the Judge Sissons Fault and the Andrew Lake Fault: it is observable on outcrops (Anand and Jefferson 2017) and is systematically intersected by drill holes (Grare et al. 2018b). Finally, the main stages of fracturing and mineralization recognized by Grare et al. (2017; 2018a, summarized in Fig. 3) at Contact include brittle tectonic activity along the Andrew Lake Fault (fracturing stage 1 or f1), development of the QB (f2), the first stage of U mineralization (f5), the second stage of U mineralization (f6), faulting associated with strong clay alteration and bleaching of the host rock (f8), and late U mineralization remobilization linked to the circulation of meteoric fluids (f9).

Methodology

Collection of structural data from field and drill cores

One hundred and forty samples were collected from drill cores obtained during 2014 and 2015 exploration campaigns by Areva Resources Canada (now Orano Canada); 28 samples came from Andrew Lake, 5 from End, 14 from Kiggavik Center Zone, 66 from Contact, and 27 from 85W (Fig. 2). In addition to classical drilling carried out during the exploration

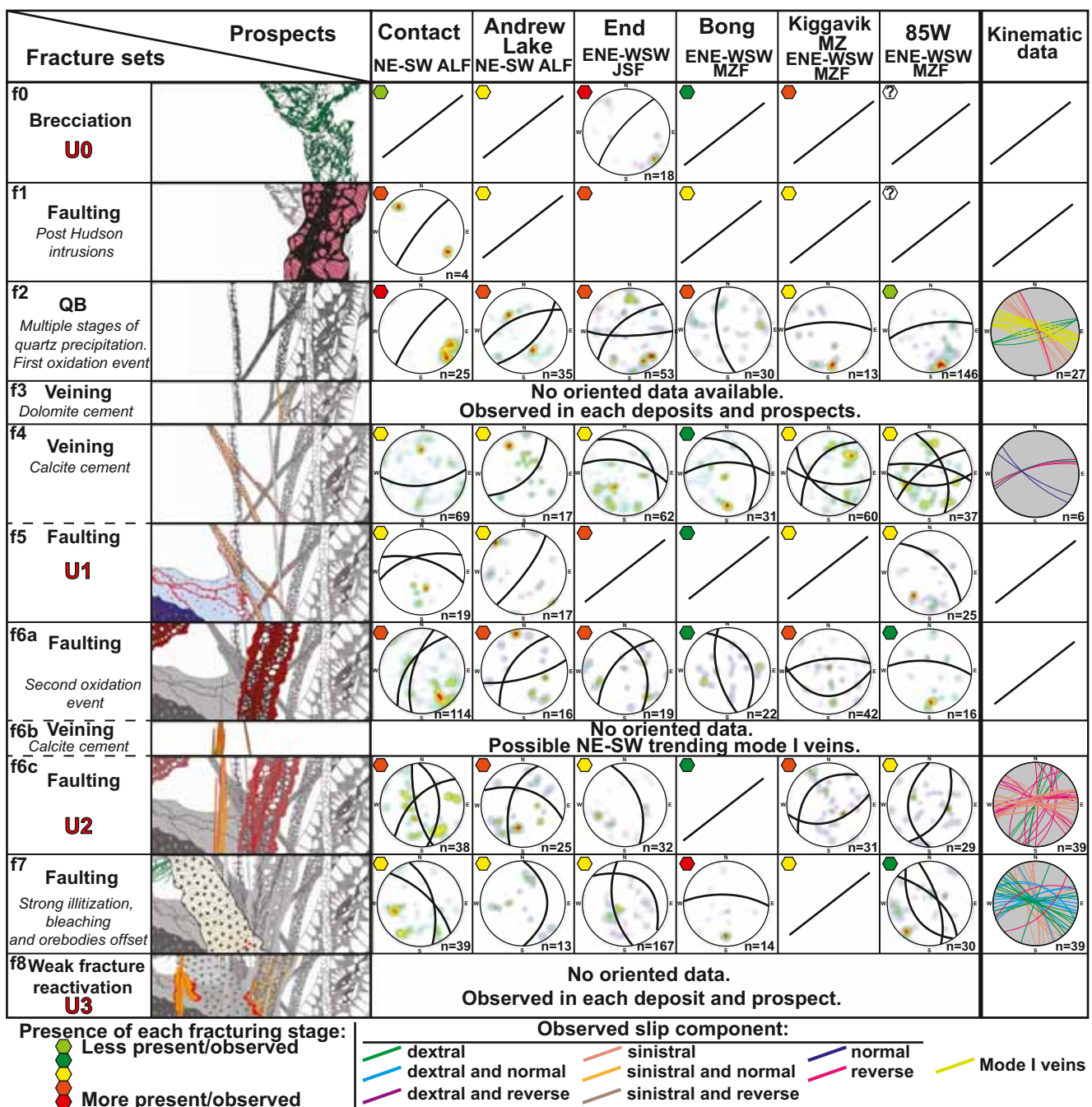


Fig. 3 Orientations of faults and breccias for each fracturing stage and for the main prospects of the Kiggavik area. The sequence of faulting/fracturing events and cross-cutting relationships are displayed on the first and second columns for reference. The presence of each fracturing stage is relative to the same fracture set or to the same prospect for the whole

Kiggavik area. The chronology of the fracturing events was presented by Grare et al. (2018a). The qualitative frequency of the fracture sets for each prospect is shown by colored symbols (e.g., f7, white clay-altered fault zones, is dominant at Bong). Schmidt's lower hemisphere stereoplots

campaigns, two double tubed exploration drill holes (CZ-15-01, at Kiggavik Center Zone, and AND-15-01 at Andrew Lake), allowing for a better preservation of the drill cores, were examined. Several drill holes (~50) from previous exploration campaigns were also described in detail (fracture orientations, cross-cutting relationships, and characterization of cements, alteration, and mineralization).

Field observations of faults, joints, and veins were made on outcrops and combined with previous field observations. Fault core zones were characterized in drill cores by the identification of breccias or gouges. Fault damage zones (Chester and Logan 1986; Wibberley et al. 2008; Faulkner et al. 2010) were documented by the associated veins (mode I or mixed mode I–mode II), joints (mode I), and undifferentiated fractures. An

“undifferentiated fracture” in this case relates to a fracture plane which cannot be unambiguously classified as vein, joint, or fault/microfault (no kinematic indicator). Fracture corridors and isolated veins, joints, and undifferentiated fractures were also systematically reported. Oriented data from Orano Canada’s Kiggavik area database were collected and processed. Orientations of ~2000 fractures and foliation planes were measured from oriented drill cores. Acoustic televiewer probing ABI40 (Williams and Johnson 2004) was run through several holes providing accurate oriented data in faulted core intervals. The mesostructural data were processed to their true orientation and plotted with Dips 6.0 software by Rocscience (see ESM 1 for detailed methodology about processing oriented data). Uncertainty on orientation measurements is usually about 10° as estimated from the comparison between oriented core-measurements and acoustic televiewer data.

Optical microscopy and scanning electron microscope

Thin sections made on veins and fault rocks were studied using a Motic BA310 POL trinocular, using transmitted and reflected lights, and a HIROX SH-3000 scanning electron microscope (SEM) equipped with a back-scattered electron detector and a nitrogen free energy dispersive spectrometer (EDS) BRK D351-10 with digital mapping capabilities at Orano (Paris, France). The SEM was operated at low accelerating voltage (10 kV), 100-nA filament current, and 600-Å beam width for a working distance between 8 and 39 mm. Complementary observations on mineralogical observations and U mineralization were performed at Service Commun de Microscopie Electronique et de Microanalyses (SCMEM) of GeoRessources lab (Vandoeuvre-lès-Nancy, France), using a JEOL J7600F scanning electron microscope equipped with an EDS.

Cathodoluminescence

The different generations of carbonate vein cements were characterized using a Technosyn cold cathodoluminescence instrument (model 8200 MkII), operating between 10- and 12-kV gun potential and between 150- and 350-μA beam current. Observations were carried out at the University of Barcelona, Spain.

Electron microprobe analysis and geothermometry of clay minerals

The chemical composition for major elements in U oxides and clay minerals (mainly chlorite and illite) were measured using a CAMECA SX-100 Electron Microprobe Analyser also at SCMEM (see ESM 1 for detailed methodology). Complementary measurements on U oxides and clay minerals (chlorite and white mica) were made on 6 thin sections with a

CAMECA SX-50 electron microprobe and conducted at the Camparis service in Sorbonne Université (Paris), based on the same analytical conditions as used at SCMEM. Temperatures were calculated from chlorite composition following the equation of Cathelineau (1988), Zang and Fyfe (1995), and Kranidiotis and MacLean (1987). White mica crystals were selected from the main altering and/or mineralization stages for electron microprobe analysis, and major element compositions (site occupancy and end-member mineral data) were used to calculate the precipitation temperatures. Temperatures were calculated following the equation of Cathelineau (1988).

Secondary ion mass spectrometry (SIMS) and LA-ICP-MS U-Pb dating and geochemical tracing of U oxides

The Pb/Pb and U-Pb isotopic compositions of U oxides was determined (see ESM 1 for detailed methodology) using a CAMECA ims 1280-HR Secondary Ion Mass Spectrometer (SIMS) at CRPG-CNRS (Nancy, France). The standard used was a uraninite sample from Zambia (concordant age of 540 ± 4 Ma; Cathelineau et al. 1990), analyzed before and after each sample for sample bracketing calibration. The $^{204}\text{Pb}/^{206}\text{Pb}$ ratio were low (< 0.00001) for the standard and unknowns, indicating that common Pb was not incorporated at the time of crystallization, except for sample 9850 ($0.000019\text{--}0.004619$). A correction for common Pb was however made for each analytical spot for all samples by precisely measuring the ^{204}Pb amount and by calculating the composition of the common Pb at the time of crystallization, based on the $^{207}\text{Pb}/^{206}\text{Pb}$ measured age and using the Pb isotopic composition calculated from Stacey and Kramers (1975) model. Ages and error correlations were calculated using the ISOPLOT flowsheet of Ludwig (Ludwig 2007). Uncertainties in the ages are reported at the 1σ level.

Rare earth element (REE: La, Ce, Pr, Nd, Sm, Eu, Gd, Tb, Dy, Ho, Er, Tm, Yb, Lu) concentrations in the different U oxides were quantified using a LA-ICP-MS system (GeoLas excimer laser (ArF, 193 nm, Microlas) coupled to Agilent 7500c quadrupole ICP-MS at GeoRessources lab) with a 16–24-μm spot size. The details regarding instrumentation and methodology are described in Lach et al. (2013).

Fluid inclusions and fluid inclusion planes

Secondary fluid inclusions (FIs) organized in fluid inclusion planes (FIPs) were studied in primary magmatic quartz (primary quartz in granite and granitic gneiss, predating all other quartz generations) from 85W and Contact using a similar approach to Mercadier et al. (2010), Wang et al. (2015), and Martz et al. (2017). The objective was to define the properties of the successive fluids that circulated through those lithologies and the related tectonic stress, as FIPs are formed during

healing of mode I microfractures. FIPs have been proposed to form perpendicular to the least principal stress axis σ_3 , i.e., in the plane that favors the maximal decrease of the total energy of the system (Lespinasse and Pêcher 1986; Gueguen et al. 1995; Lespinasse 1999; Lespinasse et al. 2005). A selection of four oriented samples was collected at 85W and Contact (only locations where oriented samples were available) and attention was paid to take samples away from main fault zones when possible in order to avoid local perturbation of the stress field. FIP dipping higher than 70° represent the majority of the FIPs in selected samples, and the study hence focuses on this group. Thus, a thin section and a wafer were prepared along a horizontal plane from selected zones of the oriented drill core in order to have a “map view” of the subvertical (dip $> 70^\circ$) FIPs. FIP orientations were measured under transmitted light microscope using the AnIma software (Lespinasse et al. 2005). More than 100 orientation measurements were done per sample, on a restrained zone ($\sim 25 \text{ mm}^2$), to generate statistically robust data.

Microthermometry was carried out on FIs from the FIPs using a Linkam® MDS600 heating-cooling stage, adapted to an Olympus® microscope at the GeoRessources lab. A total of 61 secondary fluid inclusions from FIPs were studied for microthermometry (see ESM 1 for detailed methodology).

Gas species in the vapor phase of fluid inclusions were determined at room temperature with a Labram Raman microspectrometer equipped with an Edge filter, a holographic grating with 1800 grooves per millimeter, and a liquid nitrogen-cooled CCD detector at GeoRessources (Nancy, France) (Dubessy et al. 1989).

The quantification of chemical composition (major, minor, and trace elements) of water dominated FIs was performed using the LA-ICP-MS system composed of a GeoLas excimer laser (ArF, 193 nm, Microlas) coupled to an Agilent 7500c quadrupole ICP-MS at GeoRessources lab (Leisen et al. 2012). The isotopes analyzed were ^{23}Na , ^{11}B , ^{24}Mg , ^{39}K , ^{44}Ca , ^{55}Mn , ^{57}Fe , ^{63}Cu , ^{66}Zn , ^{88}Sr , ^{55}Cs , ^{137}Ba , ^{208}Pb , and ^{238}U . The analytical precision for most elements is within 20–30% RSD (Allan et al. 2005; see ESM 1 for detailed methodology).

Results

Macroscopic texture, geometry, and kinematics of fracturing/faulting events

The approach and methods adopted in the present work are similar to those of Grare et al. (2018a). Figure 3 shows the oriented mesostructural data collected in the prospects of the Kiggavik area (except for Jane and Sleek). A detail of oriented data displaying kinematic indicators is presented in ESM 2. Together with orientation data, a statistically significant

number of kinematic indicators on veins and faults were also gathered mainly from outcrops located in different parts of the Kiggavik area, usually close to a known prospect, and also from drill cores; data are synthesized in Fig. 3. The aim is to establish whether the sequence of events recognized at Contact is also valid in the other prospects. Grare et al. (2018a) recognized 10 fracturing events at Contact among which three resulted in fracture-controlled U mineralization (Fig. 3).

Fracture stage 0 (f0) and oldest stage of U mineralization (U0, Fig. 3) This stage is named f0 and U0 in order to respect the annotation from f1 to f10 presented in Grare et al. (2018a) as it predates stage f1/U1 observed at Contact. The f0 event, unrecognized at Contact, has been identified at End, Andrew Lake, Kiggavik Main Zone, and Bong. This fracturing event is characterized by U-mineralized microbreccia usually displaying a dense network of millimeter-wide greenish microfractures (ESM 2), in breccia zones up to a 10 m thick (e.g., in End). Uranium mineralization is observed within the microfractures and is weakly disseminated within the host rock. The mineralization is usually weak but can reach several thousands of counts per second (CPS, AREVA SPPY®; i.e., 1.25 %U₃O₈ over 1 m) in some breccia zones displaying more intense fracturing. Irrespective of the grade, the brecciated and mineralized host rock is weakly clay altered. This mineralized event is cross-cut and partially overprinted by the QB (ESM 2), precluding collection of any reliable oriented data in most places. Thus, oriented data for the mineralized microbreccia are rare; however, data from End display a NE-SW trend and a steep dip to the NW. Numerous microstructures similar to solution seams are observed at the microscale and display a NW-SE to NNW-SSE orientation (data not displayed in Fig. 3).

Stage f1, pre-Thelon fracturing event (Fig. 3) At Contact, this stage is marked by faults with proto- to ultra-cataclastic fault rocks along the Andrew Lake Fault (Grare et al. 2018a), showing evidence of later silicification. These fault rocks are cross-cut by white quartz veins and mosaic breccia of QB. Because Si-bearing fluids that formed QB (f2; Fig. 3) reused pre-existing main fault zones in the Kiggavik area (e.g., ENE-WSW trending Judge Sissons Fault; Grare et al. 2018b), the related faults/fractures display variable orientation. The QB shows a NE-SW trend at Contact and Andrew Lake. Secondary ENE-WSW fracture directions are also observed at Jane and Andrew Lake. The QB displays a main ENE-WSW trend with a steep dip to the north at End and Kiggavik Main Zone. At Bong, the QB is characterized by a NNE-SSW direction and a steep dip mainly to the west and a secondary E-W direction with a steep dip to the north. At 85W, mainly small white quartz veins were observed, displaying dominant E-W directions with steep dip to the

north. Quartz veins (from QB, f2) display stepped veins, associated with (Fig. 4a) or without U oxides and arrays of mode I fractures. Stepped veins are usually trending WSW-ENE and

NW-SE (see ESM 2, 85W, Kiggavik, and St-Tropez), while mode I opening veins display a dominant WNW-ESE direction (dominantly observed at 85W).

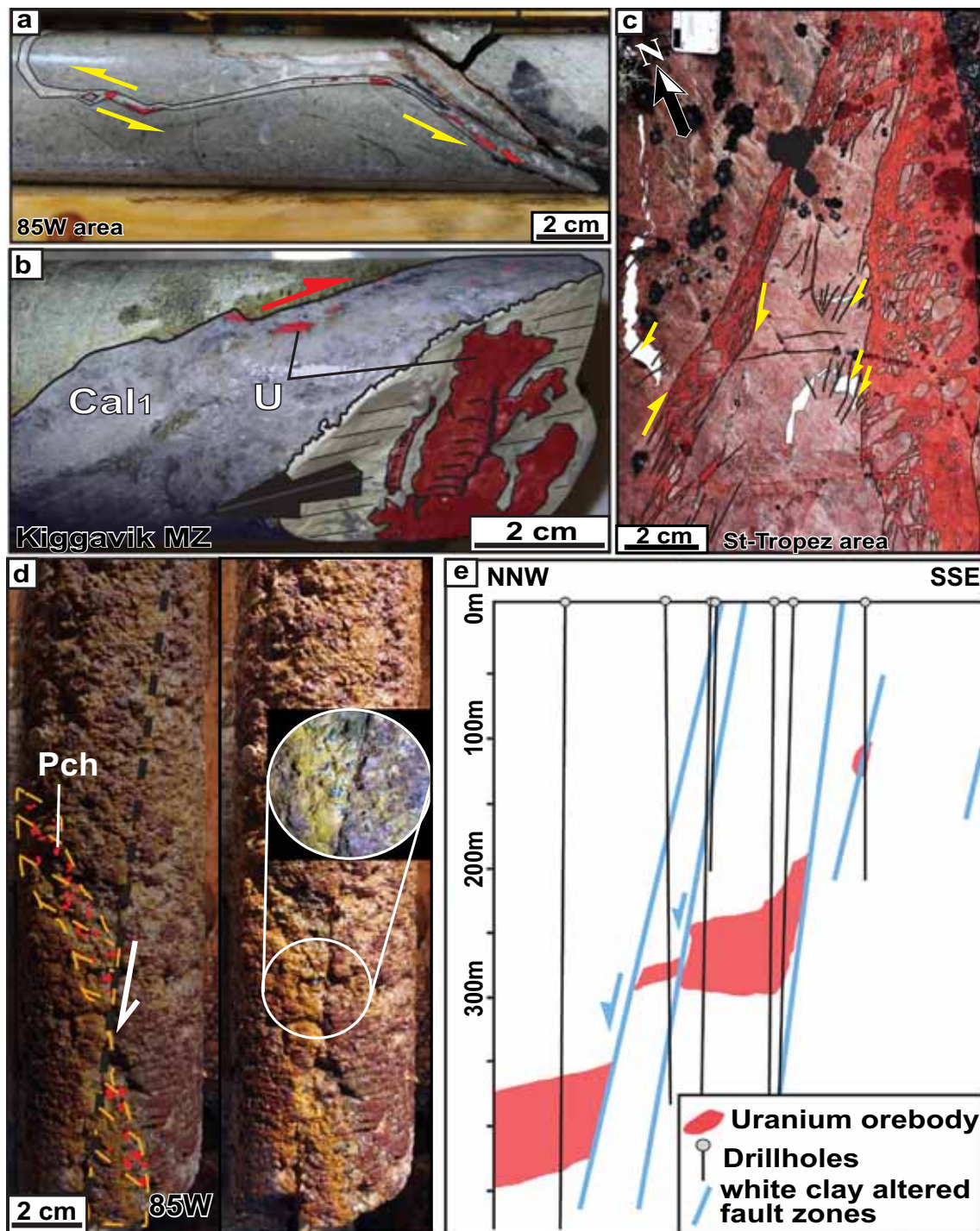


Fig. 4 a Photograph from the 85W prospect, Kiggavik area. Stepped subvertical, ENE-WSW quartz vein coated with U oxides (red) showing evidence of dextral motion. b Stepped veins of the first generation of calcite (Ca1) coated with U oxides (U1, red zones), Kiggavik area. c Photograph. NE-SW hematized fault zone (f6, cement is highlighted in red) displaying dextral kinematics (quartz veins highlighted in white). d U

oxides (U2) and a clay-cemented vein (orange outline) being cross-cut and offset by a NW-SE microfault. Host rock is strongly altered. Photographs from 85W prospect. e Simplified NNW-SSE cross-section of the Bong prospect, depicting dip-slip offset of the ore body by E-W oriented faults also driving fluids that strongly clay altered and bleached the host rock

Stage f2 (Fig. 3) This stage is observed in all prospects and generated the QB (Grare et al. 2018b), with its characteristic mosaic white quartz-sealed veins and breccia. Clasts of the QB are observed in the Thelon Formation, indicating its later reworking during deposition of the Thelon Formation. The QB is recognized along major fault zones at Bong and Kiggavik Main Zone along the ENE-WSW trending Main Zone fault, at Jane along the NE-SW trending Andrew Lake Fault and at End along the ENE-WSW trending Judge Sissons Fault. Uranium mineralization (all stages) occurs in the hanging wall and footwall of the QB but not within the breccia core. The f1 and f2 fracturing stages, and the structural control exerted by the QB on later U mineralization, were described in detail by Grare et al. (2018a, b).

Stage f3 (Fig. 3) This stage is represented by centimeter-thick dolomite veins and microbreccias, and was observed in all prospects of the Kiggavik area. The microstructures related to this stage cross-cuts the quartz veins of the QB.

Stage f4 (Fig. 3) This stage is marked by calcite-cemented (Ca1) veins and microbreccias that cross-cut the quartz veins of the QB. The veins were described by Grare et al. (2018a) as mixed mode-I mode-II shear fractures. They are observed in all prospects of the Kiggavik area, spatially associated with U-mineralized fault zones (f5). Ca1 calcite displays a yellowish-orange color under cathodoluminescence and a darker tint when closer to U oxides. Ca1 is observed as cementing microbreccias in samples from 85W and End, where U oxides coat the edges of calcite crystals. U oxides also occur as subhedral colloform shapes intergrown with the Ca1 cement, thus indicating synchronous precipitation of calcite and U oxides. Ca1 veins occur in both E-W and NW-SE directions, with conjugate dip directions. Kinematic indicators are rare but stepped veins cemented with Ca1 (f4) and U oxides (U1) were observed in drill cores (Fig. 4b). These veins display ENE-WSW and NW-SE directions.

Stage f5 (Fig. 3) This stage corresponds to the second U mineralization event (also called U1, see ESM 2). It is characterized by gray-greenish-colored, clay-altered narrow fault zones which were also observed in all prospects of the Kiggavik area. Clay alteration is characterized by illite mainly with the illitization of feldspar and chlorite through chloritization of biotite and retrograde metamorphic chlorite. This fracturing event developed strongly mineralized fault zones (e.g., 4.76 %U₃O₈ over 50 cm) with protocataclastic to cataclastic fault rocks and reopened, microfractured quartz veins from which the mineralization leaks into the foliation (see also Chi et al. 2017). At 85W, the U mineralization is completely hosted in Hudsonian granites. Due to the absence of foliation and to the coarser grain size of the minerals, the control of fractures on mineralization is stronger and easier to observe. In strongly

mineralized fault zones, where the mineralization is disseminated in the host rock, biotite is coated with pitchblende, which expands along the mineral cleavage. Like at Contact (Grare et al. 2018a), clay alteration (illitization mainly, but also chloritization) of the host rock is weak to moderate for this mineralization stage. The f5/U1 fractures follow ENE-WSW to ESE-WNW faults at Contact (Fig. 3) and are dipping to the north. At Andrew Lake, mineralization is found within N-S and E-W faults, but also within reopened and/or microfractured quartz veins trending NE-SW (f2, QB stage). At 85W, faults and minor fractures show an ESE-WNW direction, with a steep dip mainly to the north.

Stage f6 (Fig. 3) This stage is represented by deep red hematized fault zones and corresponds to the third stage of U mineralization (U2, ESM 2). It has been recognized in all prospects of the Kiggavik area. Cataclastic, strongly clay-altered (illite and chlorite) fault cores and tectonic breccias are usually not mineralized. Hematite veins, millimeter-thick calcite veins (Ca2) and microfaults host the mineralization in wide (tens of meters) fracture networks of bright red oxidized damage zones (e.g., 3.06 %U₃O₈ over 4 m). The mineralization typically spreads out into the host rock as blebs surrounded by a rim of bleaching. Clay alteration of the host rock is stronger compared to the previous stage of U mineralization. Relicts of ore minerals from previous stages can be observed where U1 fault zones are reworked by U2 faults. The calcite of Ca2 veins displays a dark orange luminescence and is observed to cross-cut U oxides of f5 stage (see ESM 2). The f6/U2 fractures (Fig. 3) are well observed throughout the Kiggavik area. At Contact, and Andrew Lake, they display N-S to NE-SW directions (i.e., the direction of the Andrew Lake Fault).

Contact is located on a W-dipping segment of the Andrew Lake Fault, while Jane and Andrew Lake are located on an E-dipping segment of the Andrew Lake Fault. The map of Fig. 2 suggests that End is likely hosted within an important relay zone of the Judge Sissons Fault where oxidized fault zones are trending mainly NNW-SSE to NE-SW (Fig. 3). At Sleek, the three main faults trends are N-S, E-W, and NW-SE, only the latter two being visible on regional maps. At Bong, 85W and Kiggavik Main Zone, the fault trends are similar to those of the QB. However, at Kiggavik Main Zone, like in Contact, an E-W trend with a shallow dip to the south is also recognized. Stage f6 fractures were observed in the field to be associated with radioactive anomalies. Mineralized fractures of f6 stage (Fig. 3) are better represented at Contact, Andrew Lake, and Kiggavik Main Zone. At Andrew Lake, U2 mineralization is characterized by ESE-WNW to NW-SE microfaults and by NE-SW millimeter-wide Ca2 veins. Ca2 veinlets are usually too thin to be measured, so reliable oriented data were obtained only at Andrew Lake. At End, U2 mineralization was guided by NW-SE to NNW-SSE faults that mainly dip to the east.

At 85W, this mineralization stage was controlled mainly by W-dipping NNE-SSW faults and by NW-SE faults as a second direction. At Kiggavik Main Zone, f6c faults trend either ENE-WSW or NW-SE to WNW-ESE. Kinematic indicators were observed in the field and in drill cores and are presented in Fig. 4. Study of relay zones in the St-Tropez area, which is located 20 km to the NNE of Kiggavik Main Zone, allowed for the interpretation of the kinematics of the fault zone (Fig. 4c). Faults with dominant E-W to ENE-WSW orientation show evidence for reverse and/or sinistral motion. Other faults with dextral indicators were also observed at Contact. The Judge Sissons Fault, trending ENE-WSW, displays a reverse-sinistral slip component (ESM 2), which postdates the main dextral normal slip component responsible of the offset of the Hudsonian granite (SLIC, Fig. 2, see also Anand and Jefferson 2017).

Stages f7–f8 (Fig. 3) These stages represent the strongest clay alteration events in the Kiggavik area, characterized by illitization, dissolution of quartz, and bleaching of the host rock. They are observed in all prospects. Numerous, un-mineralized, illitized fault zones were observed at Bong (ESM 2). These faults cross-cut mineralized fault zones (Fig. 4e) and reworked clasts bearing U oxides are observed within cataclastic fault rocks. This fracturing stage, recognized for each prospect, was extensively observed at Bong. The greenish color of some fault zones is due to the presence of reworked retrograde metamorphic chlorite and therefore does not reflect a different fracturing process; additionally, white clay fault zones (f8) are much more frequent compared to greenish clay fault zones (f7). On the basis of these new observations, we propose to gather these two fracturing events that were first presented as distinct in Grare et al. (2018a). The strongest clay alteration event is definitively termed f7. f7 fractures were recognized (Fig. 3) to be associated with NW-SE and E-W trending fault zones (e.g., 85W and End). At Bong, it is characterized by E-W trending, N-steeply dipping fault zones. These post-ore fractures display NNW-SSE direction with evidence of strike-slip sinistral motion in End and 85W areas; these faults display E-W to WNW-ESE orientation, steeply dipping to the north, with a dip-slip normal kinematics. At 85W, microfaults offset U mineralized f6 fractures (Fig. 4d). At Bong, the orebody is offset by ~E-W striking faults (Fig. 4e). The meter to tens of meters dip-slip displacement of the U orebodies appears to be greater than the strike-slip component (cm- to m-scale).

The Mackenzie diabase dykes trend NNW-SSE in the Kiggavik area. Mackenzie dykes were observed only at Kiggavik Main Zone; however, these dykes provide strong constraints on the timing of the fracturing events. The diabase dykes cross-cut the altered and mineralized fault zones (ESM 2) and are rarely fractured and altered; they can therefore be

considered having emplaced after the main tectonic and mineralization history.

Stage f8 (Fig. 3) This stage is represented by a weak reactivation of the fracture network and U redox fronts (U3) as described at Bong (Sharpe et al., 2015), Andrew Lake (Shabaga et al. 2017), and Contact (Grare et al. 2018a); they have also been recognized at End, Kiggavik Main Zone, and 85W (ESM 2). Even after careful review of drill cores throughout the Kiggavik area, it was not possible to precisely link redox fronts to specific fault zones. These remobilization fronts display the typical following succession: an oxidized (goethite), un-mineralized zone; a thin black layer where U oxides are concentrated; and a gray, reduced mineralized zone. These redox fronts are sometimes bleached by a later event described at the Contact prospect (f10), which removed iron oxides from the goethite-rich zone. It was not possible to link this final event to a specific set of fractures.

Macroscopic re-examination of prospects in the Kiggavik area therefore confirms the structural stages previously defined by Grare et al. (2018a) at Contact. As such, the sequence of fracturing events can be considered representative of the whole Kiggavik area, although changes in lithologies between the various prospects may have induced differences in the mineralogy of fault rock cements and alteration products. In addition, our approach allowed for the identification of a new stage of deformation and mineralization (f0 and U0). This initial mineralization stage is hereinafter characterized more in detail with the help of microscopic observations and geochemical data.

Mineralogy, ages of U oxides, and chemical compositions of associated clays

Mineralogy and microscopic textures of U mineralization

Samples of the U-mineralized microbreccia (f0, U0) display multiple irregular microstructures with interlocking pegs and sockets (Fig. 5a) similar to solution seams and usually surrounded by a millimeter-scale halo of quartz dissolution. These microstructures connect to microbreccias, within which millimeter clasts display irregular boundaries reflecting dissolution patterns (Fig. 5b). These microstructures are cross-cut by the QB veins (Fig. 5c and e). Electron microbeam imaging and analyses show that microfractures are cemented with iron-rich clinocllore, pitchblende (containing up to several percent of thorium), brannerite, titanium oxides, and sulfide minerals (mainly pyrite). These minerals are subhedral to anhedral mixed phases (Fig. 5d and f). Microprobe analyses show that the iron-rich clinocllore is altered into an Mg-rich chlorite (Fig. 5e), close to sudoite (ESM 3). Subhedral crystals of brannerite were observed in the same type of fractures/breccias in samples from Kiggavik Main Zone, associated

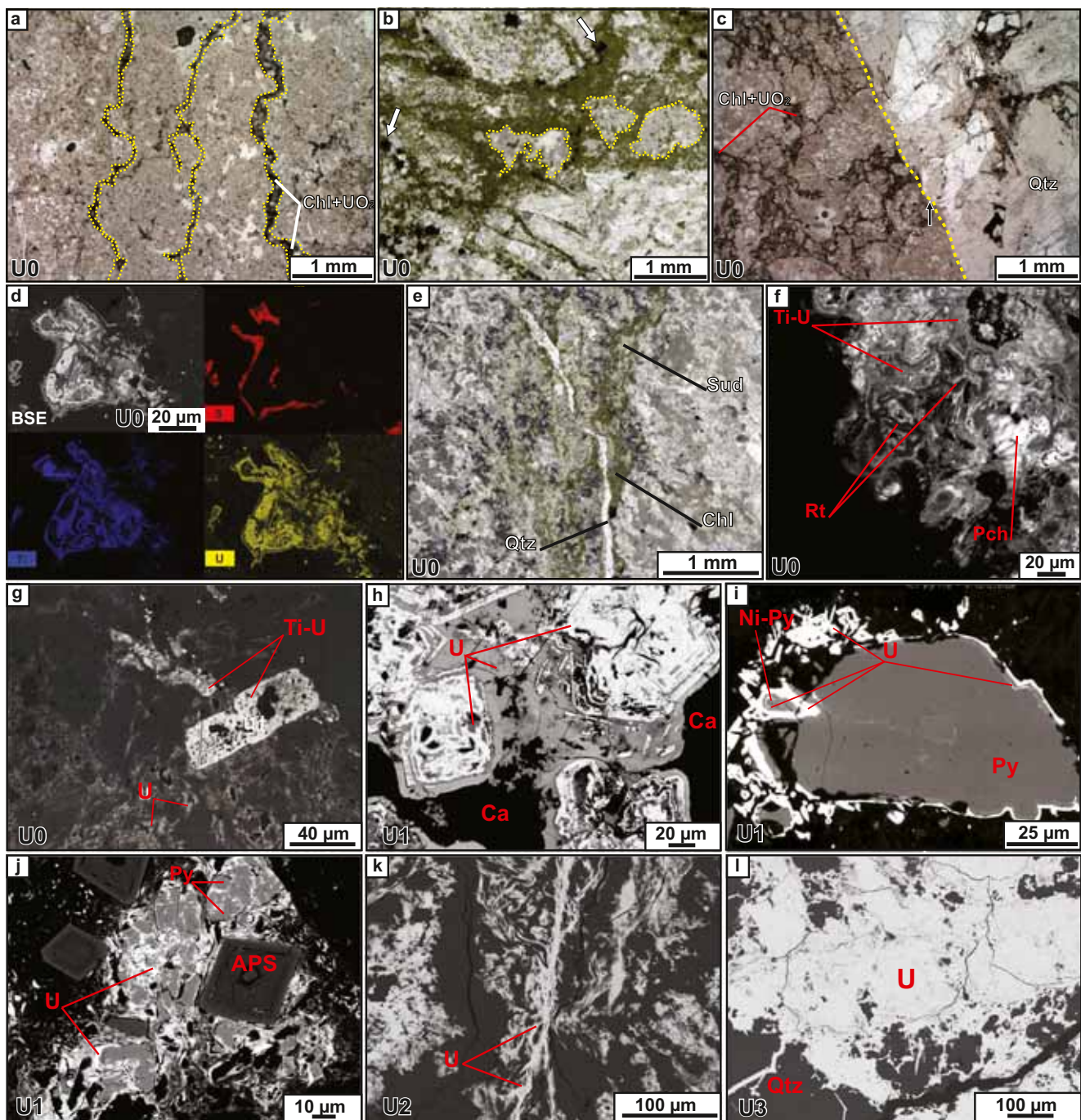


Fig. 5 Backscattered electron images of U0, U1, and U3. **a, b, c, e** Optical photomicrograph. **d, f–l** SEM pictures. **a** Undulated microstructures cemented with chlorite and U oxides. **b** Mineralized microbreccia: corroded clasts (yellow outline) cemented by chlorite and opaque minerals (opaque ore minerals indicated by white arrow). **c** Mineralized microbreccia cross-cut by a quartz (qtz) vein of QB. **d** SEM photomicrograph and element mapping of U-S-Ti compounds. **e** Microbreccia with chlorite (Chl, dark green) cross-cut by a quartz vein of QB and altered to sudoite (Sud, light green). **f** SEM photomicrograph.

Anhedral rutile (Rt), uraniferous titanate (Ti-U) and pitchblende (Pchl). **g** Microbreccia cemented with U oxides and subhedral brannerite and uraniferous titanate (Ti-U). **h** Uraninite displaying various state of alteration, cemented by calcite (Ca). **i** Ni-bearing pyrite (bravoite) and pyrite (Py) with concentric U growth zone. **j** Aluminum-phosphate-sulfate (APS) embedded in anhedral pitchblende and pyrite, in f5-U1 fault zone. **k** U2-f6 stage: anhedral pitchblende cementing anastomosing fracture. **l** U3 pitchblende coating quartz and clay minerals

with pitchblende-cemented microbreccia (Fig. 5f, g). Rutile with micro-inclusions of U oxide and coated with anhedral

U-Ti phases were also observed on samples from Andrew Lake and 85W.

Stage f5 and associated U1 is characterized by polymetallic mineralization (few f5 faults are associated with monometallic mineralization). This stage consists of pitchblende and uraninite in fractures often cemented by calcite (Fig. 5h). The U1 event is spatially associated with open quartz veins displaying colloform pitchblende along the edges, with U oxides precipitated in voids created by quartz dissolution. Bravoite-pyrite coated with pitchblende (Fig. 5i) was observed on samples from Jane, a mineralogical association also described at Contact (Grare et al. 2018a). Silver, gold, and Mo-Ni-As-Co compounds were observed in samples from Andrew Lake, End, and Kiggavik Main Zone. Anhedral Ag-U phases coating galena appear to cement microfractures; native gold is usually present as micro-inclusions within pitchblende. Aluminum phosphate sulfate (APS) minerals were observed associated with pyrite and pitchblende in a gray-greenish fault zone at 85W (Fig. 5j).

Compared to U1, f6 and associated U2 displays monometallic mineralization, characterized by pitchblende and rare sulfides (mainly pyrite). U oxides are associated with APS in oxidized rocks at 85W. Illite and sudoite were observed for both U1 and U2 mineralization stages. Anastomosing microfractures cemented by anhedral pitchblende are characteristic of this mineralization stage and were observed at Andrew Lake (Fig. 5k).

U3 is characterized by anhedral pitchblende, goethite and pyrite cementing microfractures, and coating various minerals (Fig. 5l). These new observations confirm and complement previous observations made by Chi et al. (2017), Shabaga et al. (2017), Weyer et al. (1987), and Grare et al. (2018a) at End, Andrew Lake, Kiggavik Main Zone, and Contact, respectively.

Composition and age of U oxides

Rare earth element composition

The rare earth element (REE) concentrations for U1, U2, and U3 are available in ESM 3. Figure 6a displays the chondrite-normalized patterns for samples from Andrew Lake and End. U0 oxides could not be analyzed by LA-ICP-MS due to their small size, anhedral shapes and mixing with Ti-U phases. Both U1 and U2 samples display bell-shaped chondrite-normalized patterns centered on Tb with a small anomaly in Eu (Fig. 6a). Samples are enriched in intermediate REE (Sm to Dy) compared with light REE (LREE) and heavy REE (HREE), except for sample 9850 which is enriched in LREE compared to HREE. Samples of U1 are characterized by an HREE/LREE ratio around one (9568-38 and 39) or higher (sample 9568-08). Samples of U2 are slightly depleted in LREE and their HREE/LREE ratio is therefore higher. Sample AND-15-01-05 (U2) is enriched in REE compared to the other samples. Sample And-15-01-04 (U3) displays a

stronger negative anomaly in Eu, higher concentrations in La compared to other LREE and a high LREE/HREE ratio (~ 2), comparable to sample 9850.

Sample 85W-10-04 (Fig. 6a) displays a different pattern compared to the other samples of the Kiggavik area with a much higher concentration of REE (up to a factor 10). The pattern displays a positive slope from La to Sm, and then a negative slope to Lu. Such a signature has never been described before in the Kiggavik area.

U-Pb isotopic composition and absolute age dating

Uranium oxides studied for REE concentrations were also analyzed by SIMS for U-Pb isotopic dating (see ESM 3). The dated samples come from Andrew Lake (4), End (1), and 85W (1). Based on macroscopic characteristics and mineralogical associations, samples 9850, 9568-39, 9809, and 85W-10-04 are interpreted to belong to U1, samples 9851 and And-15-01-05 to U2, and sample And-15-01-04 to U3.

The data plot along or below the discordia in the $^{206}\text{Pb}/^{238}\text{U}$ - $^{207}\text{Pb}/^{235}\text{U}$ Concordia diagrams (Fig. 6b), which suggests that most of the samples have lost Pb since U oxide crystallization. Electron microprobe analysis shows that uraninite and pitchblende display relatively high U contents (~ 75 – 86 wt%) and low Pb contents (0–5 wt% on average, ~ 10 wt% for one sample) especially for U1 and U2, indicating also a loss of Pb. Three samples from Andrew Lake yielded upper intercept ages (ESM 3) at 347 ± 58 Ma (sample 9850) and 344 ± 19 Ma (9851) for U1, 565 ± 38 Ma (And-15-01-05, anchored at 0 ± 10 Ma) for U2, and 547 ± 13 Ma (And-15-01-04) for U3. The sample from 85W yields an upper intercept age at 1073 ± 5 Ma (85W-10-04). The samples from End yields upper intercept ages at 1277 ± 10 Ma (9568-38), 1175 ± 23 Ma (9568-39), and 1257 ± 58 Ma (9809).

Composition and crystallization temperatures of chlorite and illite

Chlorite

Chlorite from the Kiggavik area falls into three types: retrograde metamorphic chlorite, chlorite (altered and unaltered) associated with U0 mineralization, and chlorite associated with U1 and U2 mineralization. The compositions are presented in a chlorite ternary diagram in Fig. 7a (Velde, 1985). Composition of chlorite associated with U0, U1, and U2 are presented in ESM 3.

Representative compositions of chlorite analyzed from U mineralized microbreccia samples (f0, U0) are plotted in Fig. 9 and chlorite cement analyzed from the microbreccia are shown in Fig. 7c. Representative cation proportions (based on 14 oxygens) of unaltered chlorite

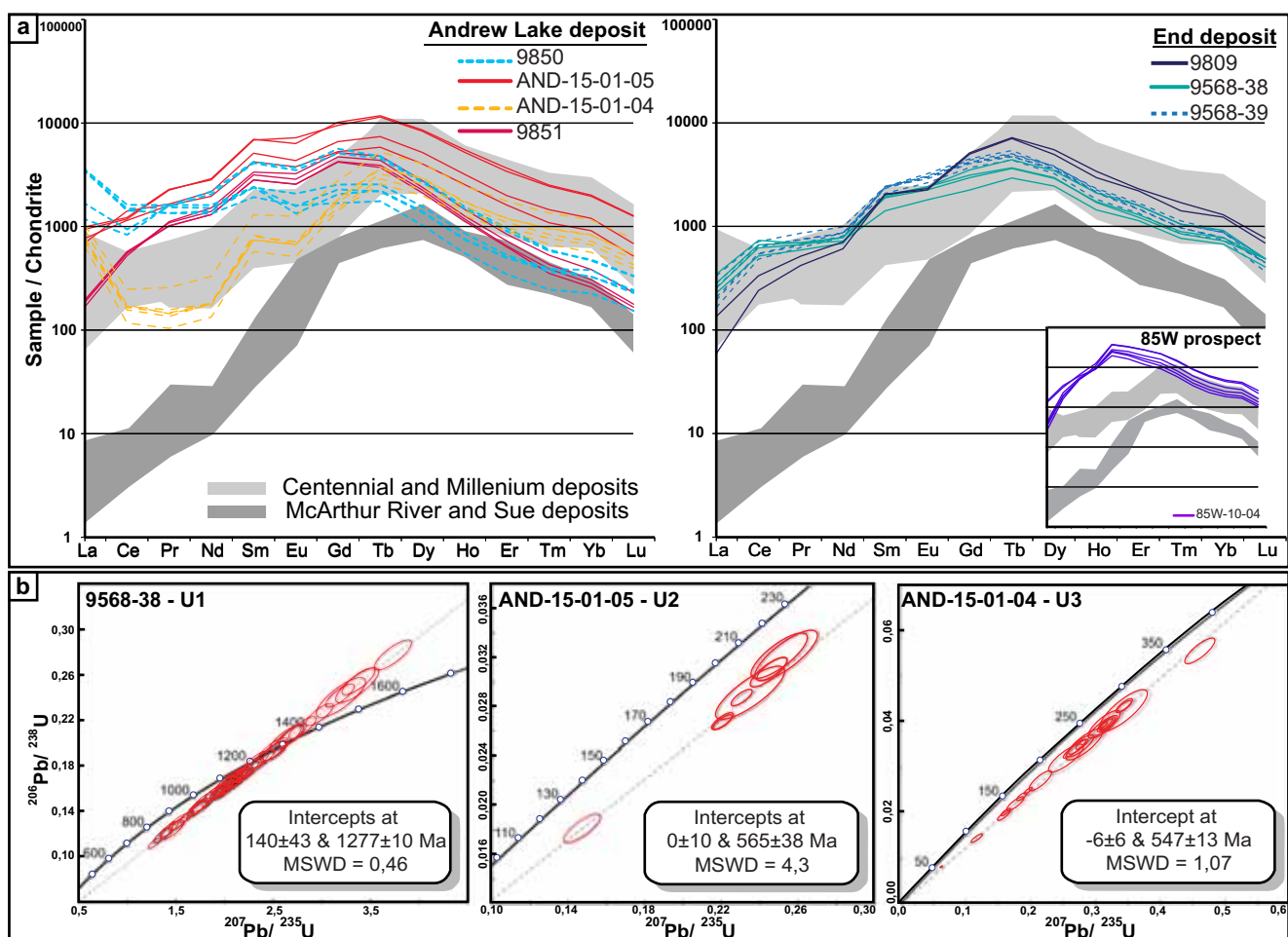


Fig. 6 **a** Chondrite-normalized REE patterns for pitchblende and uraninite from 8 different samples from Andrew Lake (left), End (right), and 85W (small insert). Each curve corresponds to an in situ SIMS or LA-ICP-MS REE analysis in a selected U oxide of the studied samples. Ages for the samples were obtained in this study (see also Fig. 10), except for sample 9568-38 and 9568-39, obtained by Lach et al. (2013). The gray zones correspond to the unconformity-related U oxide reference

chondrite-normalized REE patterns from the Mc Arthur River and Sue Deposits (Mercadier et al. 2011b), Centennial and Millenium deposits (Alexandre et al. 2015). **b** $^{206}\text{Pb}/^{238}\text{U}$ - $^{207}\text{Pb}/^{235}\text{U}$ Concordia diagram showing the isotopic composition of U oxides (pitchblende and uraninite) from three samples coming from End (9568-38) and Andrew Lake (And-15-01-05, And-15-01-04). Analytical data are in ESM 3

associated with U0, together with calculated temperatures, are in ESM 3, and indicate an iron-rich species of trioctahedral chlorite. The octahedral occupancy is close to 6 atoms when the structural formulae are calculated with total Fe in the ferrous state and the Fe/(Fe+Mg) ratio is generally close to 0.5. Structural formulae of chlorite linked to U1 and U2 plot toward the sudoitic end member (di-trioctahedral chlorite, Fig. 7b, in ESM 3), characterized by an Al-Mg-rich composition and an octahedral occupancy close to 5 cations. Sudoite was also characterized through XRD by Pacquet (1993a, b, c). Numerous analyses of chlorite associated with U0 reveal a mixture of variable amounts of iron-rich chlorite and sudoite, showing that neofomed dioctahedral chlorite, co-genetic with U0, was altered to di-trioctahedral chlorite. This is consistent with petrographic observations showing dark green chlorite surrounded by light green chlorite (Fig. 7c).

Crystallization temperature were calculated using several methods, only for the Fe-rich chlorite variety linked to U0, as the geothermometers cannot be applied on low- T° di-trioctahedral chlorite such as sudoite. The Cathelineau (1988) and Jowett (1991) thermometers returned temperatures ranging from 295 to 333 °C whereas Kranidiotis and MacLean (1987) and Zang and Fyfe (1995) thermometers returned temperatures ranging from 130 to 159 °C.

Illite and mica

Representative compositions of white micas associated with pre-Umin alteration (pre-U0), with U1-f5 and U2-f6 mineralization stages and late clay alteration micas (f7) are detailed in ESM 3 and plotted on ternary diagrams representing the average compositional fields of dioctahedral mica-like phases (Dubacq et al. 2010; Fig. 7d). Pre-U mineralization (f1)

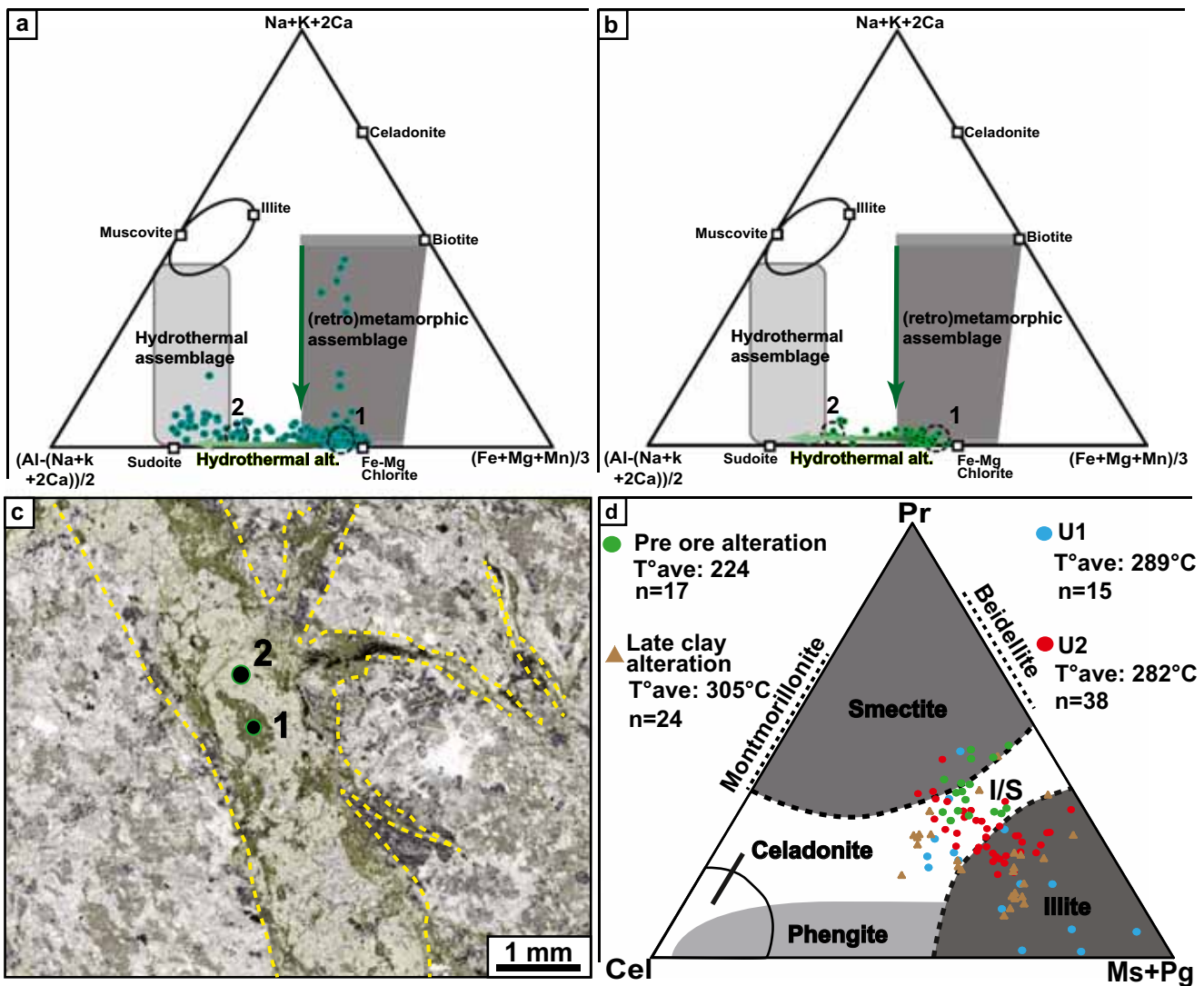


Fig. 7 **a** Ternary diagram of chlorites from different locations in the Kiggavik area (Jane, Contact, 85W, Andrew Lake). **b** Ternary diagram representation of chlorite formed during U0 mineralizing stage and their later hydrothermal alteration. Structural formulas of chlorites were plotted in a MR3-2R3-3R2 diagram (Velde 1985). **c** Photomicrograph of a U0 microbreccia cemented with unaltered dioctahedral chlorite (1. dark

green), altered to light green di-trioctahedral chlorite (2. sudoite). Opaque minerals are ore minerals. Numbers localize the point analyzed with EMPA, which are plotted in B. **d** White mica plotted on a ternary diagram of the average compositional fields of dioctahedral mica-like phases, after Dubacq et al. (2010). Pr: pyrophyllite; Cel: celadonite; Ms.: muscovite; Pg: paragonite

alteration is characterized by interlayered illite/smectite and smectite. Most of the white mica alteration characteristic of U1 and late ore clay alteration consist of illite. White mica characterizing U2 is represented by illite and interlayered illite/smectite. The distribution of the data points in the diagram likely indicates inheritance of illite from muscovite/sericite.

Crystallization temperatures calculated using the equation of Cathelineau (1988) return an average of 224 °C for pre-U mineralization alteration, 289 °C for U1, 282 °C for U2, and 305 °C for f7 (Fig. 7d). Calculation of temperatures using the Battaglia (2004) method yielded similar results. The temperature differences between the two methods for a given sample are generally within 10 °C.

Composition of fluid inclusions and orientations of fluid inclusion planes

Composition of fluid inclusions

Two types of fluid inclusion planes (FIPs) were identified based on the nature of constitutive fluid inclusions (FIs): type 1 and type 2 FIPs (Fig. 8a). Rare FIPs present FIs that characterize type 1 and type 2 FIPs; they are labeled “mixed FIP” (Fig. 8a) and were not studied further.

Type 1 FIPs are represented by monophasic, vapor-only, and dark fluid inclusions, rounded, with rare “negative crystal” shape (Fig. 8b). Their size varies from 3 to 10 μm. No phase change was observed for these FIs when

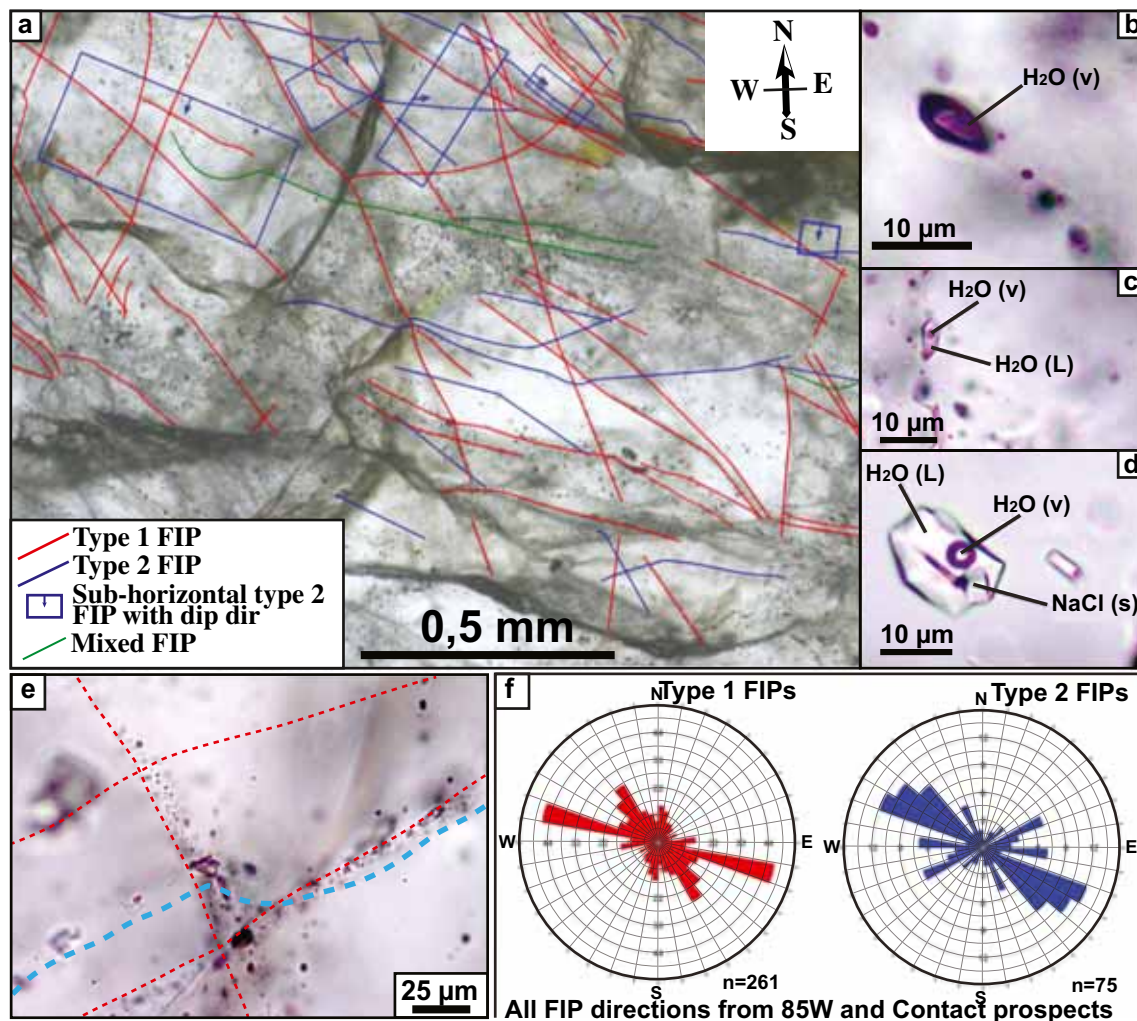


Fig. 8 Thick-section photomicrograph. **a** Magmatic quartz from the granite of 85W displaying monophase FIPs cross-cut by aqueous FIP. **b** Monophase fluid inclusion displaying negative crystal shape. **c** Biphasic aqueous fluid inclusion. **d** Triphase aqueous fluid inclusion with halite

crystal. **e** Monophase FIPs (red dotted lines) and aqueous FIPs (blue dotted line). Monophase FIs are obliterated at the intersections between monophase and aqueous FIP. **f** Synthesis of all FIP, detailed oriented data are in ESM 2

cooled to $-190\text{ }^{\circ}\text{C}$. Analysis of the gas phase by Raman spectroscopy indicates that the FIs are filled with H_2O vapor.

Type 2 FIPs are represented by biphasic and triphase aqueous FIs. At room temperature, biphasic FIs are characterized by a dominant liquid aqueous phase with a vapor phase representing in most cases ca. 10% of the FIs by volume (Fig. 8c). They have variable shapes with a size varying from 3 to 20 μm . H_2 , O_2 , CH_4 , and N_2 were occasionally detected in trace amounts in the vapor phase of the biphasic fluid inclusions by Raman spectroscopy. Triphase FIs are characterized by a dominant liquid aqueous phase with a vapor phase representing in most cases ca. 10% and display a cube of halite (Fig. 8d). They have variable shapes and their size range from 6 to 20 μm . H_2 and O_2 were occasionally detected in trace amounts in the vapor phase of the triphase inclusions using Raman spectroscopy. Type 1 FIPs are cross-cut by type 2 FIPs (Fig. 8e).

A summary of microthermometric data obtained for the analysis of biphasic and triphase FIs ($n = 61$) is given in ESM 3. The FIs have been classified according to the nomenclature of Derome et al. (2005), also used by Richard et al. (2016) and Martz et al. (2017) in order to allow for a better comparison (refer to ESM 1). Over two third of FIs belong to the Lw' or Lwh' types that are typical of the so-called CaCl_2 -rich brine (Derome et al. 2005). They show high salinity (25.3 to 39.3 wt% eq. $\text{NaCl} + \text{CaCl}_2$), T_h from 62 to $>215\text{ }^{\circ}\text{C}$ (no further heating to avoid decrepitation) and T_s NaCl generally higher than T_h (120 to 235 $^{\circ}\text{C}$) for Lwh'. About 15% of the FIs belong to the Lw1 or Lwh types that are typical of the so-called NaCl -rich brine (Derome et al. 2005). They show slightly lower salinities (22.2 to 31.3 wt% eq. $\text{NaCl} + \text{CaCl}_2$), T_h of 126 $^{\circ}\text{C}$ and T_s NaCl close to T_h (129 $^{\circ}\text{C}$). The remaining 15% of FIs belong to the Lw'' type that is typical of the so-called low-salinity fluid (Derome et al. 2005). They show variable and relatively low salinity (2.3 to 16.8 wt%

eq. $\text{NaCl} + \text{CaCl}_2$), and T_h systematically over 220 °C, possibly related to the frequently high volume of vapor phase, up to 60% (no further heating above 220 °C to avoid decrepitation).

The concentrations of several major, minor, and trace elements in aqueous fluid inclusions (mainly Lw' and Lwh' inclusions) were measured by LA-ICP-MS. The absolute contents of every element analyzed display a large range of values (Fig. 9), the highest being represented by Ca (31,000 to 80,000 ppm), Na (5600 to 38,000 ppm), K (3500 to 17,000 ppm), Mg (1200 to 14,000 ppm), Fe (from 5900 up to 11,200 ppm), and Sr (1000 to 6700 ppm). Metals such as Ba (590 to 14,000 ppm) and Pb (270 to 11,000 ppm) display moderate concentrations. Zinc (270 to 800 ppm), U (6 to 350 ppm), Cu (<80 to 400 ppm), Rb (37 to 140 ppm), and Cs (23 to 40 ppm) display lower concentrations compared to other elements. The FIs are characterized by high concentrations in Ca compared to Na, indicating that FIs studied are dominated by a CaCl_2 -rich brines.

Orientations of fluid inclusion planes

Strike of subvertical fluid inclusion planes are plotted as rose diagrams in Fig. 8f. The FIPs at 85W are mainly type 1 (186 FIP measurements out of 240). In drill hole 85W-09 (samples 85W-09-07 and 85W-09-04), type 1 FIPs display main directions of N100–110. Secondary directions are N10–30 and

N120–140. Type 2 FIPs returned a main direction of N110–120 and secondary directions around N120–130 and N040–060. For drill hole 85W-10 (sample 85W-10-04B), type 1 FIPs display main directions around N350–010, N140–160, and N110–130. Type 2 FIPs have main directions around N060–080 and N120–140. At 85W (ESM 2), the main direction for type 1 FIPs is N100–110, and the two minor directions are N350–010 and N140–160. Some sub-horizontal FIPs were observed at 85W; they are mainly composed by triphase FI. Type 2 FIPs show two directions: N110–140 and N040–080.

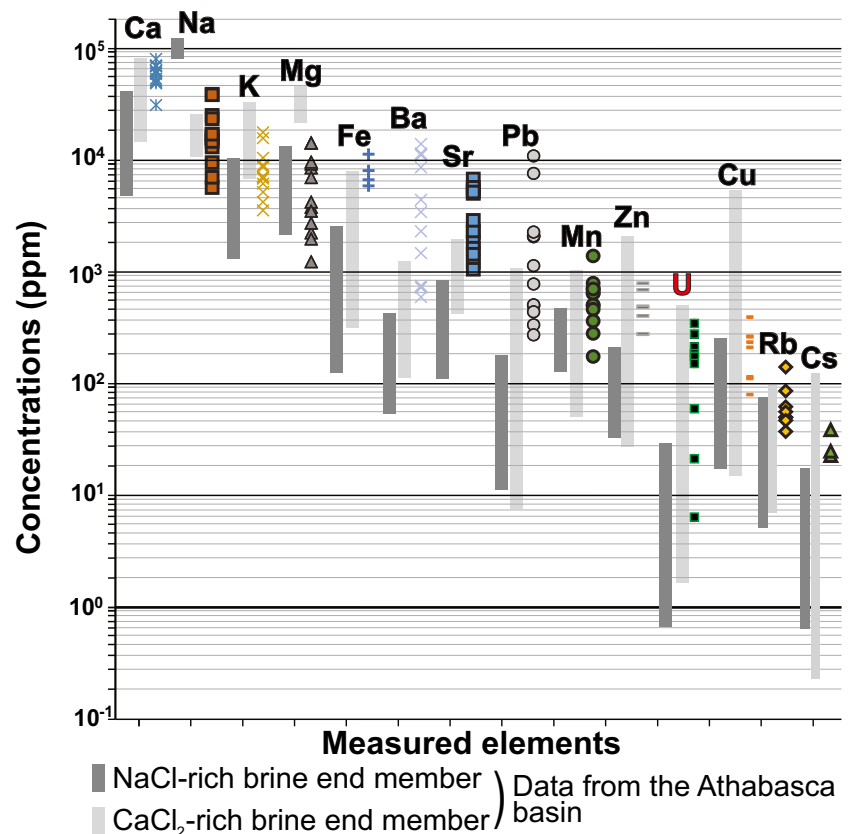
At Contact, type 1 FIPs were also the most represented type (75 FIP measurements out of 96); these FIPs display a main N130–150 direction, secondary N110–130 direction, and minor direction of N000–020. Aqueous biphasic and triphase FIPs overprint type 1 FIPs like at 85W. Type 2 FIPs display two directions: N110–120 and N80–N100. The FIP directions were also compared with reference to the sub-constant N10/10° E orientation of the granitic gneiss foliation at Contact.

Discussion

Evolution of temperature of mineralizing fluids

UO is associated with chlorite crystallizing from 130 to 159 °C up to 295–333 °C, depending on the method of calculation

Fig. 9 Concentration (ppm) in several metals for selected fluid inclusions in the Kiggavik area (CaCl_2 -rich basinal brines). Comparison is made with data from the Athabasca Basin; Richard et al. 2010, 2016



used. The evaluation of iron valence, thus the amount of Fe^{3+} , directly impacts the calculation of the temperature and has always been an analytical challenge. However, Bourdelle and Cathelineau (2015) demonstrated that the lower the temperature, the lower the impact of Fe^{3+} and a model based solely on Fe^{2+} is suitable in terms of practicability and simplicity while still giving reliable results. In our study, the high temperatures (295–333 °C) obtained using Cathelineau (1988) and Jowett (1991) methods for dioctahedral chlorite of this stage appear consistent with the presence of brannerite and the high Th contents of pitchblende in U0. A similar high Th content was also described by Weyer et al. (1987) at Kiggavik Main Zone. The incorporation of thorium (Th^{4+}) into the uraninite structure is indeed correlated with the temperature and is commonly observed in metamorphic or magmatic uraninite, which form at $T > 300$ °C, contrary to hydrothermal U oxides which form at $T < 300$ °C (Depiné et al. 2013; Mercadier et al. 2013; Frimmel et al. 2014; Cuney et al. 2015). The pre-Thelon high-temperature dioctahedral chlorite cementing f0 fractures would have likely been altered to sudoite at a later time, probably after the deposition of the Thelon Formation, by the circulation of Thelon-derived basinal brines thus crystallizing lower temperature di-trioctahedral chlorites (~100–200 °C).

The circulation of such basinal brines is considered to be related to the formation of U1 and/or U2. Calculating the temperature of formation of sudoite is not possible, precluding any comparison with temperatures obtained by illite thermometry. Pre-U1/f5 white mica that crystallized at low temperatures (~220 °C in average) could represent either early localized alteration along fault zones (f1) during development of the earlier Baker Lake and Wharton basins, or circulation of diagenetic fluids from the Thelon Basin. White mica synchronous with U1 and U2 returned temperatures of ca. 280–290 °C, but slightly higher in the case of U1. These temperatures are higher than those typically obtained for illite in the Athabasca Basin (220–280 °C, Ng et al. 2013; Chu and Chi 2016), which could indicate crystallization of illite and URU oxides at greater depth, and/or under a higher geothermal gradient for the Thelon Basin compared to the Athabasca Basin. A higher geothermal gradient, linked to magmatism associated with emplacement of the Kuungmi lavas at 1540 ± 30 Ma (Chamberlain et al. 2010), i.e., the age proposed for the emplacement of U1 (Sharpe et al., 2015), is our preferred hypothesis, as no geological process could explain an increase in depth of crystallization. A similar explanation was proposed by Chi et al. (2018) in order to reconcile elevated temperature recorded by FIs and shallow URU mineralization in the Athabasca Basin: they proposed the potential occurrence of a magma chamber underneath the basin.

Homogenization temperatures obtained by microthermometry on type 2 FIPs (syn-/post-Thelon event) range from 62 to > 220 °C. These temperatures are

comparable to those obtained in the Athabasca Basin for diagenetic-hydrothermal fluids (Derome et al. 2005; Richard et al. 2016), and at End (100–300 °C, Chi et al. 2017) from fluid inclusions in quartz spatially associated with post-Thelon uraninite and calcite in the Kiggavik area.

The shift of ~100 °C between temperatures given by fluid inclusions and those given by illite geothermometry has already been reported in the Athabasca Basin by Chu and Chi (2016). Such a difference could be related to the fact that the T_h measured for the fluid inclusions represent the minimum value for the trapping temperature. However, pressure correction of the fluid inclusion data does not completely explain the difference in temperature (Richard et al. 2016; Chi et al. 2018).

Post-ore illite alteration, observed in f7 fractures, returned higher temperatures of 290–350 °C. This increase in temperature could be linked to the emplacement of large volumes of magma associated with the giant dyke swarm of the Mackenzie event (Ernst et al. 1995; Hou et al. 2010). This magmatic event could have triggered the circulation of “hot” hydrothermal fluids shortly before emplacement of the diabase dykes and sealing of the faults, which would also be consistent with illite Ar-Ar ages obtained at ca. 1300 Ma at End, Andrew Lake, Kiggavik Main Zone, and Bong (Ashcroft et al. 2017; Shabaga et al. 2017; Fig. 10).

Typology of U mineralization

REE signatures

The chondrite-normalized REE pattern of U oxides is usually considered to be specific to each type of U prospect and to directly reflect its conditions of formation (temperature, redox conditions, fluid composition, REE source(s); (Mercadier et al., 2011a, b; Frimmel et al. 2014; Alexandre et al. 2015)). The U oxides from End (U1) and Andrew Lake (U2) display an overall bell-shaped REE pattern centered on Tb which is typical of URU systems (Bonhoure et al. 2007; Mercadier et al., 2011a, b; Eglinger et al. 2013; Alexandre et al. 2015). Such patterns were also obtained by Fayek et al. (2017) at Kiggavik Main Zone and unambiguously indicate that U1 and U2 at Kiggavik area crystallized under physico-chemical conditions similar to U oxides from the Athabasca Basin URU prospects (Pagel 1975; Derome et al. 2005; Richard et al. 2010; Martz et al. 2018). Some U oxides however present modified bell-shaped REE patterns compared to unaltered samples from URU prospects of the Athabasca Basin, with enrichment in LREE, while concentrations of HREE remain the same (Fig. 6a). This modified bell-shaped REE pattern, observed for U oxides in remobilization fronts in the Kiggavik area (Fig. 8a), was first described by Mercadier et al. (2011a) for U oxides in a remobilization front at the Eagle Point U prospect in the Athabasca Basin, and is

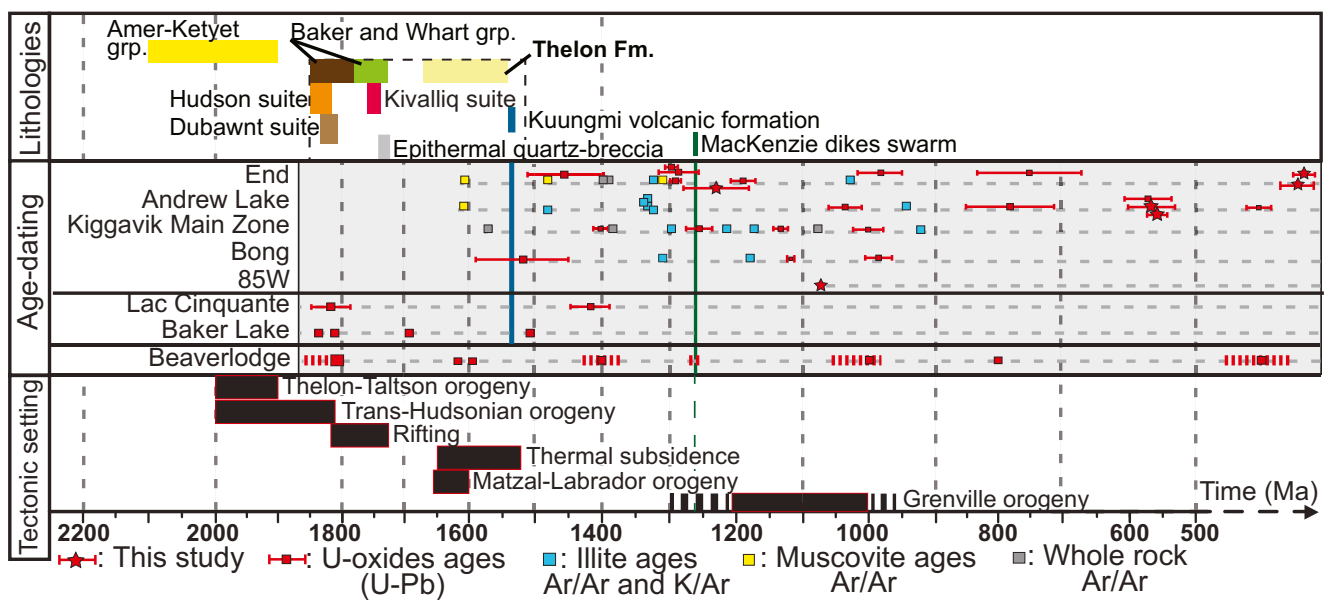


Fig. 10 Summary of ages within the Thelon/Baker-Lake area, through U-Pb isotopes on U oxides (Farkas 1984; Miller et al. 1986; J. Bridge et al. 2013; Lach et al. 2013; Sharpe et al. 2015; Chi et al. 2017; Shabaga et al. 2017; this study), Ar-Ar ages on illite (Friedrich et al. 1989; Riegler 2013;

Ashcroft et al. 2017; Shabaga et al. 2017), Ar-Ar on muscovite (Ashcroft et al. 2017; Shabaga et al. 2017), K-Ar on illite (Friedrich et al. 1989) and whole rock analysis (Hunt and Roddick 1988, 1992a, b)

interpreted to be linked to the interaction between primary UO_2 and low-T ($< 50^\circ\text{C}$) meteoric water. Such modified spectrum is observed for U1 and U2 from the Kiggavik area (Fig. 6a) and indicates that these initial U generations were chemically affected by meteoric water. This is consistent with their reset U/Pb isotopic ages (younger than 600 Ma; Fig. 6b) and with macroscopic observations of redox fronts containing goethite that formed in low-T and low-salinity conditions (Mercadier et al. 2011a). Such alteration and/or remobilization of brine-related U oxides by late low-T meteoric waters appears to be a common and widespread feature in the Kiggavik area, based on published and present data (Sharpe et al., 2015; Shabaga et al. 2017).

A REE pattern similar to the one obtained for the 85W sample has only been previously described for a U oxide from Zambia (Eglinger et al. 2013), which was considered an URU prospect. Such a pattern is however not characteristic of URU oxides, as observed for all prospects in the Athabasca basin (Mercadier et al. 2011b; Alexandre et al. 2015). The REE composition and the age (post-Mackenzie dyke) of this U oxide indicate that the conditions for the crystallization of these U oxides were different than U1 and U2 U oxides, but are still unknown.

Fluid inclusion compositions

Dense arrays of dark FIs (type 1 FIPs) cross-cut by syn/post Thelon high-salinity inclusions have been described previously in the Athabasca Basin (Mercadier et al. 2010; Wang et al. 2015; Pascal et al. 2016; Martz et al. 2017). However, those

inclusions were dominated by CO_2 , CH_4 , and N_2 and interpreted as retro-metamorphic fluids equilibrated with graphite-rich lithologies. Here, the vapor-dominated aqueous inclusions could be explained by boiling of an aqueous fluid that could be linked to a pre-Thelon epithermal event, which has been characterized in/close to the Kiggavik area (Turner et al. 2001; Grare et al. 2018a, b). A similar event was also proposed for the Athabasca Basin (Chi et al. 2018). Therefore, considering that type 1 FIPs are cross-cut by type 2 FIPs, it is much more likely that these trends of vapor-rich FIs characterize the QB event. In addition, the absence of CO_2 , CH_4 , and N_2 could be linked to lack of graphite-rich lithologies in the Kiggavik area. H_2 and O_2 observed in FIs from type 1 and type 2 FIPs indicate radiolysis of H_2O in presence of U (Dubessy et al. 1988; Richard 2017).

In type 2 FIPs, the occurrence of similar FI types as described in Derome et al. (2005) and Richard et al. (2016) attests to the presence of NaCl-rich and CaCl_2 -rich brines and a low-salinity-fluid at 85W. Such brines have been observed throughout the Athabasca Basin for the URU deposits. The characteristics of FIs described here show many similarities with those described at End by Chi et al. (2017). The major difference here is that no fluid unmixing was observed. Therefore, fluid unmixing observed by Chi et al. (2017) is probably related to a different fluid episode than that associated with type 2 FIPs. Temperatures and salinity of brine inclusions are higher than those obtained by Renac et al. (2002) in the Thelon sandstone away from mineralized zones: 100–160 $^\circ\text{C}$, ca. 17 wt% NaCl. The brines are thought to be primarily derived from evaporated seawater (Richard et al.

2011, Richard et al., 2013, Richard et al., 2014). The CaCl_2 -rich brines have been proposed to reflect interaction of NaCl-rich brine with the basement rocks (Derome et al. 2005; Mercadier et al. 2010; Richard et al. 2010, 2016; Martz et al. 2018). In this study, we observed dominantly CaCl_2 -rich brine FIs, which would reflect important interaction of the basal brines with basement rocks. The slightly higher temperatures measured for the CaCl_2 -rich brines in the Thelon Basin, compared to the Athabasca Basin, in line with the temperatures calculated for illite, could indicate a higher thermal gradient or a deeper percolation of brines within the basement. This could have well been the case in the Kiggavik area where the mineralization formed at an unconstrained depth in the basement rocks, below a now eroded cover of unknown thickness.

Brine inclusions display similar major and trace element concentrations compared to NaCl-rich and CaCl_2 -rich brines from the URU deposits in the Athabasca Basin (Richard et al. 2010, 2012, Richard et al., 2013, Richard et al., 2016; Martz et al. 2018), being extremely rich in U, Zn, Rb, Sr, Cs, Ba, and Pb. It is noteworthy that Mg is particularly low compared to the Athabasca basin and that boron was not detected, which is in line with the lack of Mg-tourmaline noted in the Kiggavik area compared to the Athabasca Basin. The data therefore indicate that metal-rich (in particular U-rich) and highly saline basal brines circulated in the basement rocks of the Kiggavik area and formed U1 and U2 at ca. 1500–1275 Ma, in agreement with the REE pattern for unaltered U oxides of these two mineralizing stages.

Metallogenic model of the Kiggavik area

The combination of all structural, mineralogical, fluid inclusion, dating, and geochemical characteristics of the different U prospects from the Kiggavik area allows proposing a structurally controlled metallogenic model of U mineralization. The main faulting/fracturing events, the related tectonic stress, and the fracture network evolution are presented in synthetic block diagrams (Figs. 11, 12, 13, 14, and 15). These block diagrams were built for Bong, Kiggavik Main Zone (both located on ~ENE-WSW trending faults), Andrew Lake, and Contact (both located on ~NE-SW trending faults).

Pre-Thelon Basin faulting/fracturing events and the first stage of U mineralization (magmatic type U0)

(f0, U0) The first U mineralization event was recognized in all major prospects in the Kiggavik area. U0 is characterized macroscopically by microbrecciation (f0) of the host rock and is better preserved at greater depth. Hydrothermal rutile cementing microfractures and coated with pitchblende at Contact (Grare et al. 2018a) are interpreted to be relicts of this first mineralization stage. Solution seams characteristics of this stage are traditionally observed in sedimentary

environments (e.g., Rutter 1983; Benedicto and Schultz 2010) but have also been described in igneous rocks, for example in rhyolite and welded tuffs (Donald Bloss 1954; Burma and Riley 1955; Golding and Conolly 1962). Mineralized microfractures and the characteristic solution seams were also described by Miller (1980) and LeCheminant et al. (1979) in their study of the Kazan Fall U mineralization in the Baker Lake basin. Kinematic indicators associated with f0/U0 are represented by solution seams oriented NNW-SSE (Fig. 11). These solution seams likely indicate a roughly WSW-ENE trending σ_1 consistent with what was proposed by Hadlari and Rainbird (2011) for the formation of the Baker Lake basin. Major faults (Andrew Lake Fault, Judge Sissons Fault, Main Zone Fault, probably Thelon Fault) were active at that time (Fig. 11a), probably under WSW-ENE σ_1 and NNW-SSE σ_3 (Fig. 11b), and mineralized. The prevalence of this mineralizing stage in prospects controlled by major ENE trending faults highlights the role played by major fault zones in focusing both fracturing events and fluid circulations through time for the Kiggavik area.

The f0/U0 is cross-cut by quartz veins of the QB (inferred to have formed at ca. 1750 Ma) and ages of ca. 1830 Ma were obtained on pitchblende within the Baker Lake Basin by Miller and LeCheminant (1985) and Bridge et al. (2009, Fig. 10). Such mineralization event is plausible in the Kiggavik area, since a breccia pipe of the Christopher Island formation (ca. 1833 Ma; Rainbird et al. 2006) was observed in the eastern part of the Kiggavik area, along with ultrapotassic minette and bostonite dykes (Anand and Jefferson 2017) of the Dubawnt igneous suite. These lithologies are enriched in U (LeCheminant et al. 1987; Miller and Blackwell 1992; Peterson et al. 2011) and represent a potential source of U. It is inferred that the U0 mineralization event occurred in the Thelon-Baker Lake area at the end of the Trans-Hudsonian orogeny (ca. 1830 Ma), in response to retro-arc extension with deposition of the Baker Lake formation and emplacement of U-rich peralkaline magmas of the Dubawnt igneous suite (Cuney 2014; Cuney et al. 2015). This U mineralization event is the first one in the Kiggavik area and is likely of magmatic origin. U0 constitutes the first significant “stock” of U oxides in the Kiggavik area that will be later remobilized. U0 is observed in significantly mineralized brecciated rocks, and would have been an easily available source of U for basal brines during their circulations in basement structures along with possible other U sources, to form the younger U mineralization. The presence of a pre-Thelon-basin source of U is comparable to what is described near the Athabasca basin: volcanic and metasomatic U in the western margin (Dieng et al. 2013, 2015) or magmatic and metamorphic U described in the eastern margin (Mercadier et al. 2013). Secondary U sources in the Kiggavik area could have been the metamorphosed epiclastic rocks of the Puqik Lake formation

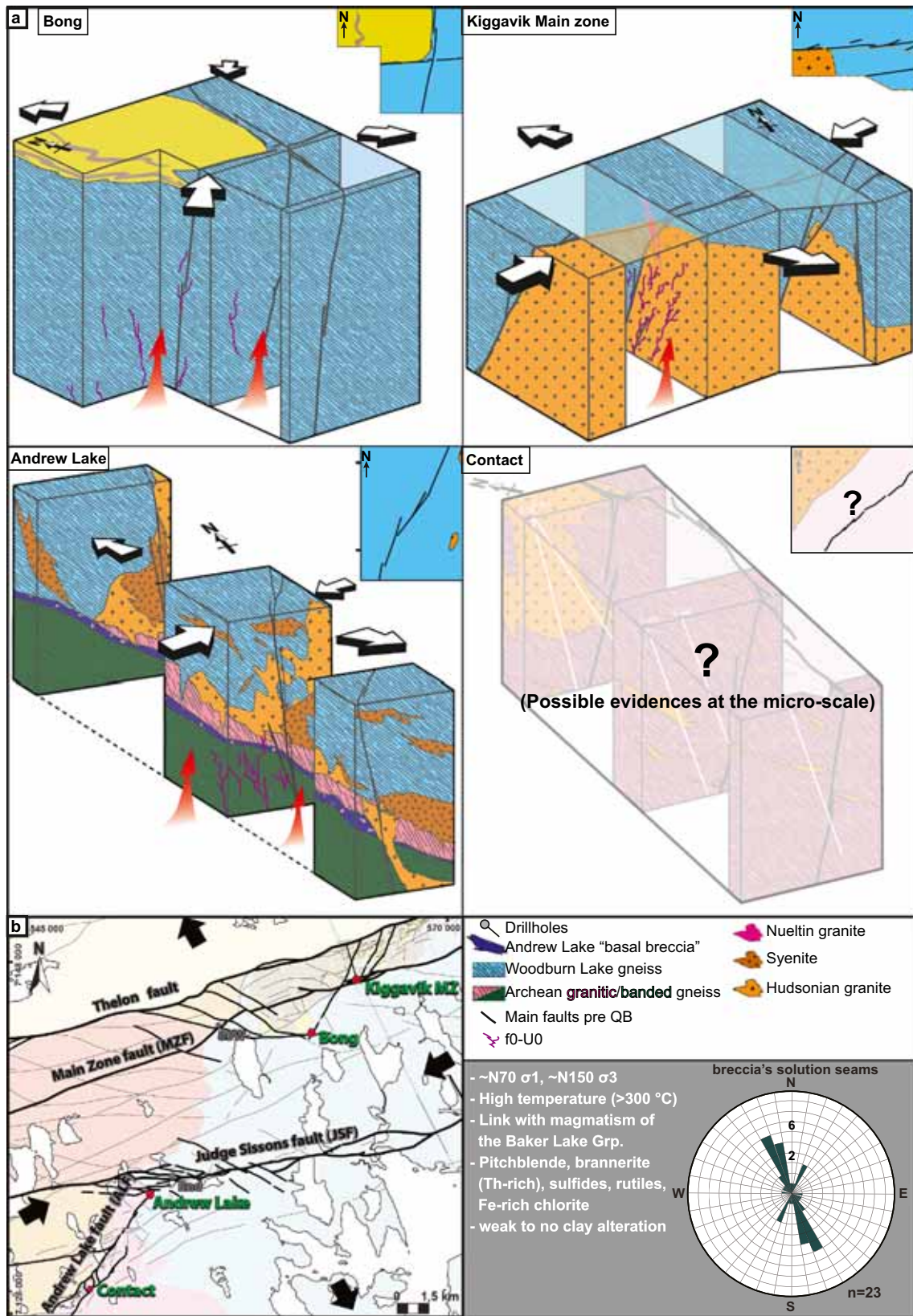


Fig. 11 Pre-Thelon basin first stage of microbrecciation and U mineralization in the Kiggavik area associated with magmatism of the Kivalliq igneous suite. **a** Bloc diagram. **b** Map view of the fracture network at this stage

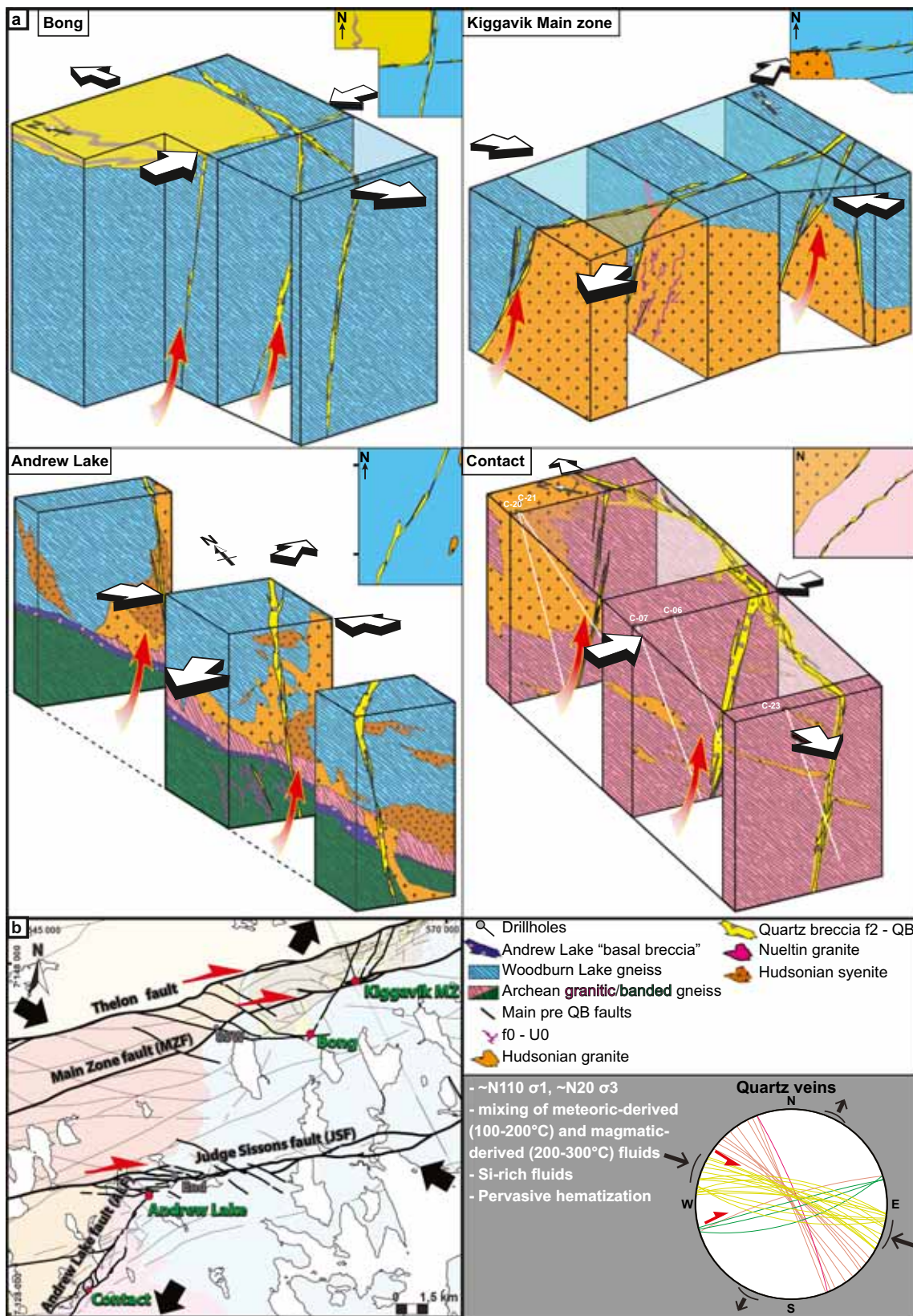


Fig. 12 F2/QB. Pre-Thelon hydraulic quartz breccia linked to magmatism of the Kivalliq igneous suite (ca. 1750 Ma). ESE-WNW oriented σ_1 and NNE-SSW oriented σ_3 . **a** Bloc diagrams for Bong,

Andrew Lake, Kiggavik Main zone, and Contact prospects. **b** Map view of the fracture network at this stage

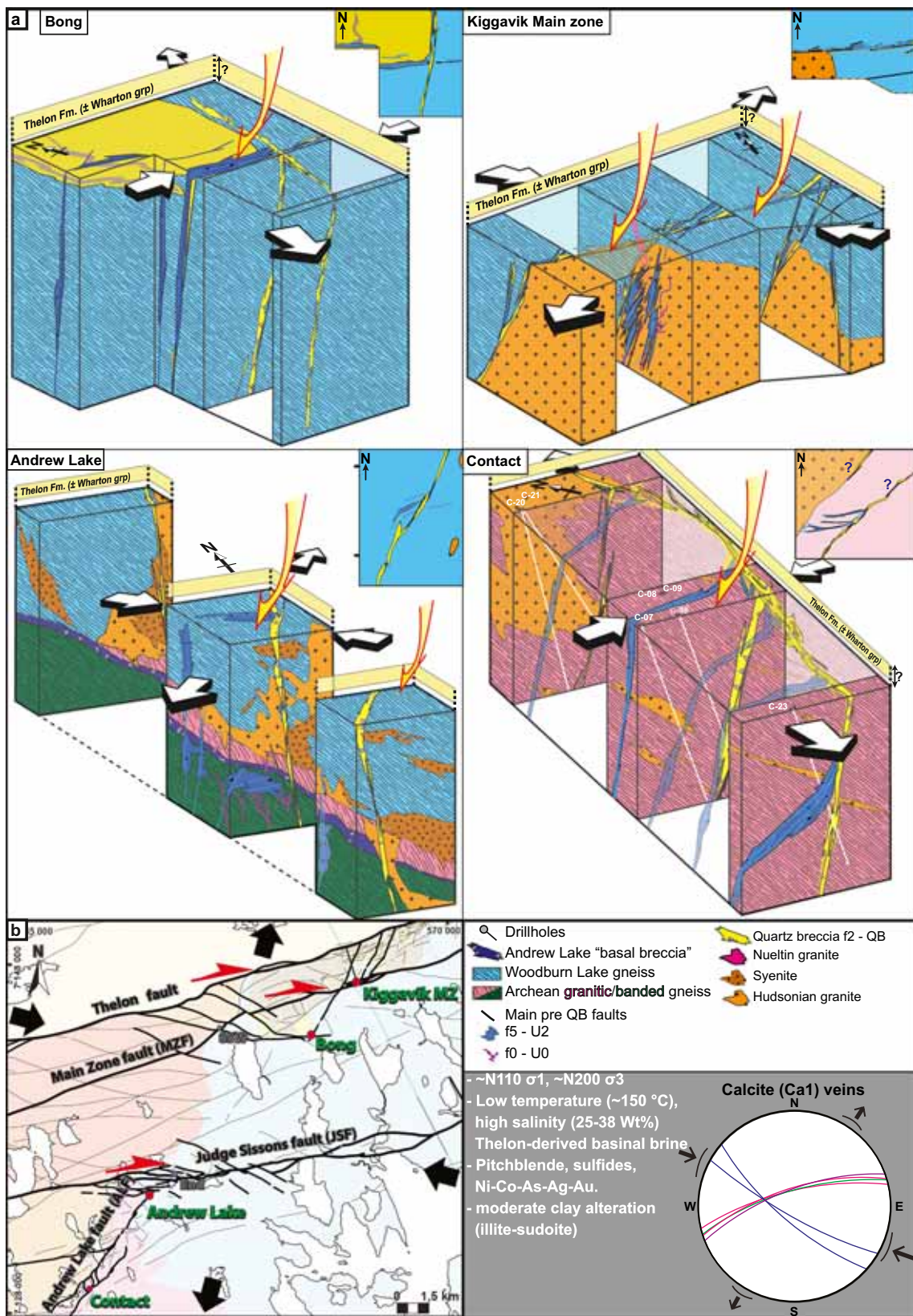


Fig. 13 F5/U1. Syn-Post-Thelon circulation of basinal brines. ESE-WNW oriented σ_1 and NNE-SSW oriented σ_3 . **a** Bloc diagrams for Bong, Andrew Lake, Kiggavik Main zone, and Contact prospects. **b** Map view of the fracture network at this stage

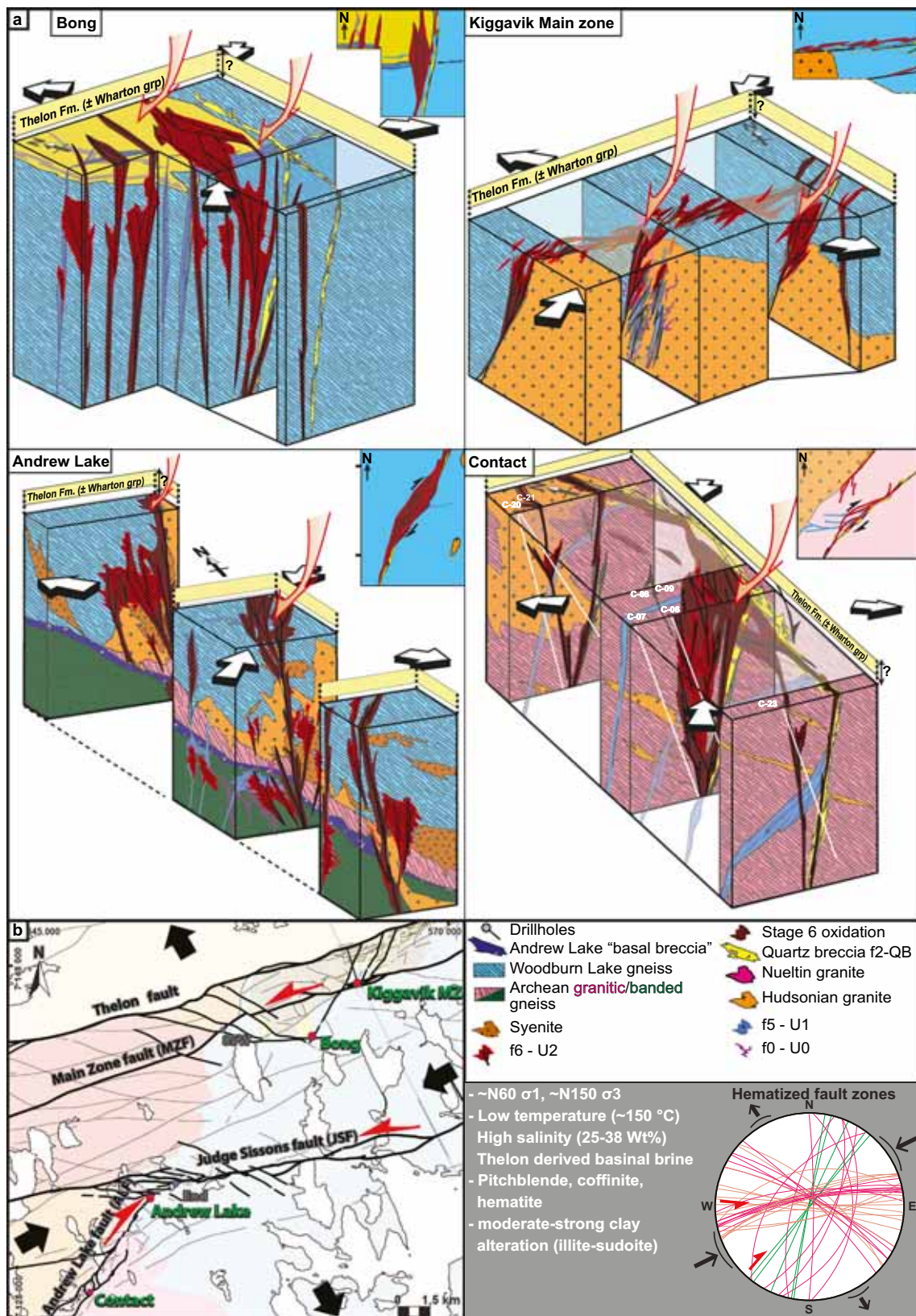


Fig. 14 F6/U2. Post-Thelon renewed circulation of basal brines. ENE-WSW oriented σ_1 and NNW-SSE oriented σ_3 . **a** Bloc diagrams for Bong, Andrew Lake, Kiggavik Main zone, and Contact prospects. **b** Map view of the fracture network at this stage

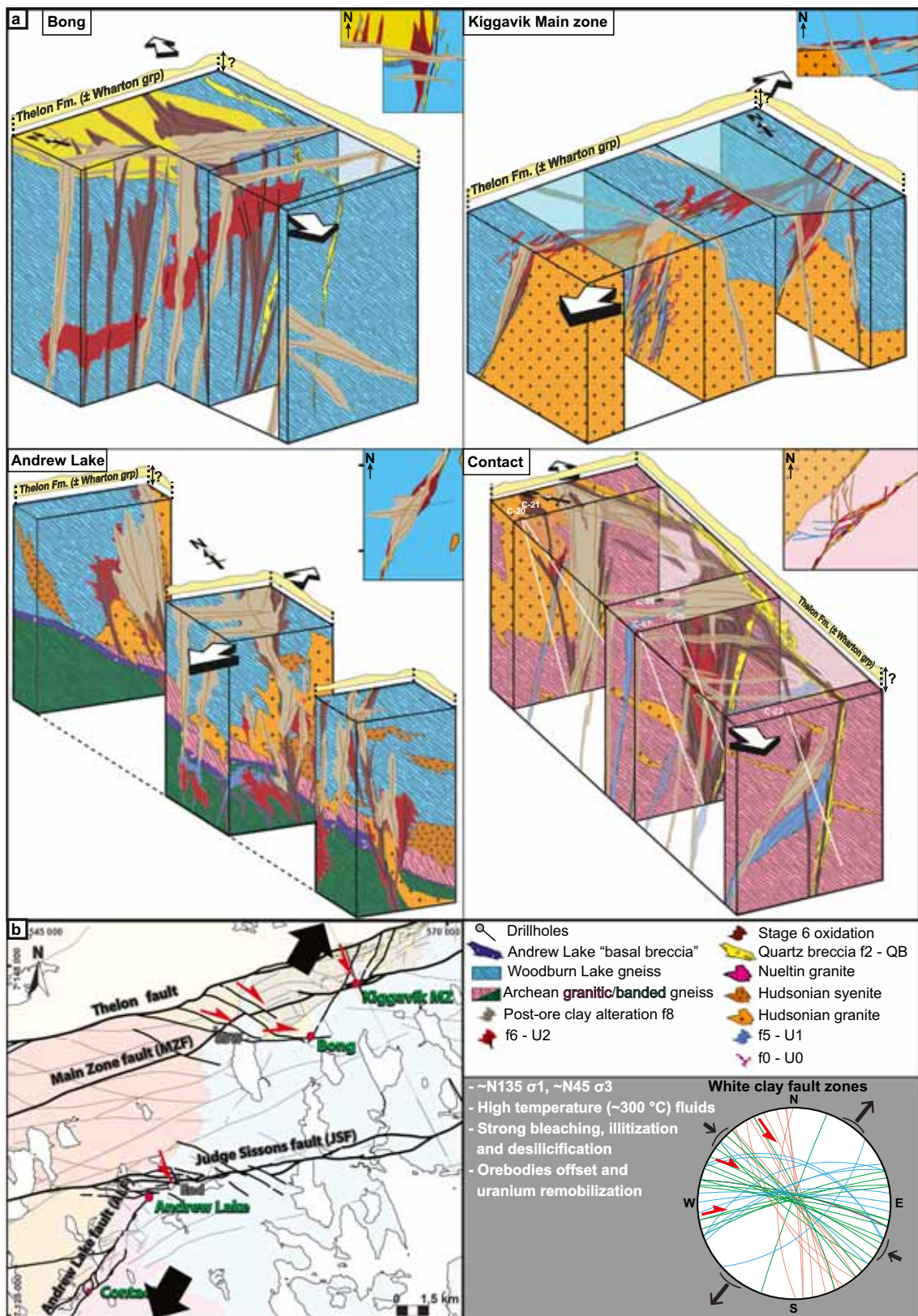


Fig. 15 Post ore, Pre Mackenzie dykes (1267 Ma) illitization and desilicification, local remobilization, and offsetting of orebodies. NNE-SSW oriented σ_3 . a Bloc diagrams for Bong, Andrew Lake, Kiggavik Main zone, and Contact prospects. b Map view of the fracture network at this stage

(Johnstone et al. 2017), rhyolitic flows of the Wharton group (Blake 1980; Peterson et al. 2015), bostonite dykes of the Dubawnt igneous suite (ca. 1830 Ma; LeCheminant et al. 1987; Miller and Blackwell 1992; Peterson et al. 2011), U-rich pegmatite of the KIS (Scott and Peterson 2012), and U-rich minerals such as monazite (Hecht and Cuney 2000; Richard et al. 2015).

(QB, f2) Intense quartz brecciation related to the QB event (linked to magmatism of the KIS dated at ca. 1750 Ma; Peterson et al. 2015; Grare et al. 2018b) occurred along major fault zones (i.e., Main Zone fault, Judge Sissons Fault, Andrew Lake Fault) in the Kiggavik area and also south of this area (Baudemont and Reilly 1997; Turner et al. 2001). Circulation of high-temperature, low-salinity fluids was focused along major faults and relay zones (Fig. 12a), silicifying previously formed fault rocks. The formation of the QB occurred under a likely stress regime with WNW-ESE trending σ_1 and NNE-SSW trending σ_3 (Fig. 12b). The silicification event controlled, at least partly, later fracturing and fluid circulation, depending on the thickness of the quartz breccia. The most fractured and silicified part of the QB (i.e., the breccia core) behaved as a transverse barrier for fluids but enhanced along-strike fluid migration and entrapment through reopening of veins along its outer boundaries. The QB played therefore a major role in partitioning fracturing and fluid flow during the later U mineralization stages (Grare et al. 2018a, b).

(Syn?) Post-Thelon faulting/fracturing events: second and third stages of U mineralization (URU-type U1 and U2)

(f5, U1) This stage is characterized by monometallic to polymetallic mineralization within reduced narrow fault zones (Fig. 13a). With the exception of Contact, the f5 stage reflects the orientation of the main fault zones in which they are hosted (NE-SW trend of the Andrew Lake Fault for the Andrew Lake prospect, WNW-ESE trend of the Main Zone fault for the 85W prospect). Illite is the main alteration product but sudoite was observed in altered mineralized fault rocks at Jane (Miller 1997), End (Lida 1997), Bong, (Riegler et al. 2014; Sharpe et al. 2015), and Kiggavik Main Zone (Pacquet 1993a). Aluminum phosphate sulfate minerals, synchronous with U mineralization, were observed at 85W (this study), and by Riegler et al. (2016) at Bong.

U1 postdates quartz veins and dolomite veins precipitated from highly saline, basin-derived brines (Chi et al. 2017 and Riegler, 2013; respectively), and is synchronous with the first generation of stepped calcite veins. Fluid inclusions in calcite were studied by Chi et al. (2017) at End. Although not characterized using cathodoluminescence, it is likely that this calcite material was made of Ca1 (as defined in our study) because veins of the second generation are usually too thin for a reliable study of fluid inclusions. This indicates that Ca1

precipitated from Thelon-derived highly saline basinal brines. The synchronicity between Ca1 and U1 suggests that faulting/fracturing stage f5 associated with U1 corresponds to a stress regime with WNW-ESE σ_1 and NNE-SSW σ_3 (Fig. 13b). Such a stress regime is consistent with type 2 FIPs that display dominant WNW-ESE trends (Fig. 8f) indicating a NNE-SSW to NE-SW trending σ_3 . The WNW-ESE trending σ_1 is further consistent with the dextral slip component along E-W to ENE-WSW trending fault relay zones in the QB and with WNW-ESE trending type 1 FIPs. This is also in agreement with the observations made by Anand and Jefferson (2017) who concluded that reactivation of ENE-WSW, north-dipping extensional faults (such as the Thelon Fault or the Judge Sissons Fault) occurred under a \sim N110–140° trending σ_1 . The oldest ages for U have been obtained by Farkas et al. (1984) and Sharpe et al. (2015) at 1403 ± 10 Ma and 1520 ± 79 Ma, respectively. Absolute ages obtained in this study for U1 are between 1293 ± 08 and 1187 ± 20 Ma for End prospect and 354 ± 47 Ma at Andrew Lake. Local heating and circulations of hydrothermal fluid associated with emplacement of the Kuungmi lavas at ca. 1540 ± 30 Ma (Chamberlain et al. 2010) are described as one possible first event of URU-type mineralization in the Kiggavik area (Sharpe et al. 2015). This age was observed throughout the Thelon-Baker Lake area (Turner et al. 2003; Bridge et al. 2013). Ages at 1500–1400 Ma are comparable to ages obtained on oldest URU mineralization in Athabasca (1514 ± 18 Ma, Cumming and Krstic 1992; 1519 ± 22 Ma, Fayek et al. 2002; 1540 ± 19 Ma, Alexandre et al. 2009). The time frame defined by age-dating studies and the reconstructed stress regime are consistent with the Racklan orogeny that occurred to the west of the Kiggavik at ca. 1600–1380 Ma (Cook 1992; Cook and MacLean 1995; Thorkelson 2000). This orogeny would be at the origin of the WNW-ESE shortening, as proposed by Anand and Jefferson (2017).

The ENE-WSW, north-dipping faults formed earlier during the deposition of the Baker Lake and Wharton Groups were reactivated at that stage with a dextral-normal kinematics, favoring the circulation of the NaCl-rich basinal brines from the Thelon Basin down to the basement rocks and the probable formation of CaCl₂- and U-rich mineralizing brines (U1). Minerals fingerprinting highly saline basinal brines (sudoite, APS), fluid inclusion characteristics (metal-bearing, high salinity, Ca-rich, T_h between 100 and 220 °C), and REE bell-shaped patterns of U oxides, along with the timing of the mineralization event (post-Thelon Formation), support the conclusion that U1 precipitated from Thelon-derived basinal brines, and is thus of unconformity-related type, like the U deposits in the Athabasca Basin.

(f6, U2) This stage is characterized by monometallic mineralization within reddish oxidized fault zones (Fig. 14a, b). As already pointed out by Grare et al. (2018a) at Contact, these

oxidized faults are not always mineralized and fault cores that display strong clay alteration are usually not mineralized. Uranium mineralization is stronger in well-developed, moderately clay-altered damage zones. These observations are in line with the classical view of fault zones (Chester and Logan 1986; Kim et al. 2004; Faulkner et al. 2010) where fracturing and fluid flow are more important in damage zones than in core zones of faults (Caine et al. 1996). The orientations of U₂-bearing faults do not necessarily reflect the orientations of the main faults that host the mineralization. Mineralized U₂ faults display a complex range of orientations, sometimes with antithetic dip to the main fault. These variable orientations are typical within damage zones linking main faults and has been described in a variety of settings (Kim et al. 2004; Rotevatn and Bastesen 2014; Fossen and Rotevatn 2016).

Minerals specific to URU mineralization were observed associated with U₂: APS minerals were observed in oxidized fault zones at Contact (Grare et al. 2018a) and 85W (this study), and sudoite associated with illite was described, at Contact (Grare et al. 2018a), Jane (Miller 1997), Kiggavik Main Zone (Hasegawa et al. 1990), End (Lida 1997), and Andrew Lake (Hasegawa et al. 1990; Pacquet 1994). Along with hematization of the host rock, the mineralogical differences (e.g., absence of Ni-Co Arsenides) between U₁ and U₂ highlight that U₂-bearing fluids had a different composition (although still being basal brines) than U₁-related fluids, with slightly higher f_{O_2} and pH (see Pourbaix diagram in Romberger 1984). This difference may be explained by the evolution of the fracture conduits through time, since this new faulting/fracturing event formed new fractures while likely reactivating the complex, pre-existing fracture network of the Kiggavik area.

The response of the fracture network to the newly applied tectonic stress was obviously different depending on its orientation: at Andrew Lake and Contact, hematitized and mineralized damage zones of faults trending NE-SW are well developed in contrast to those associated within ENE-WSW fault zones of the Kiggavik Main Zone prospect (Fig. 14a). The f₆ fault zones underwent sinistral and/or reverse movements (Fig. 14). Sinistral reactivation of the ENE-WSW Judge Sissons Fault overprinted, in some places, the dextral motion on this fault that offsets the Schultz Lake Intrusive Complex. These observations, together with the NE-SW crack-seal calcite (Ca₂) veins (f₆) coated with U₂ spherulitic pitchblende support a local stress regime with NE-SW to ENE-WSW trending σ_1 and NW-SE to NNW-SSE trending σ_3 for this tectonic event. This stress regime may account for the secondary NE-SW to ENE-WSW trends of type 2 FIPs (Fig. 8f) associated to a second episode of circulation of basal brines. The regional meaning of this stress regime however still remains poorly understood.

In terms of timing, the f₆ faults cross-cut the sandstones of the Thelon Formation (Grare et al. 2018a). In addition, cross-cutting relationships indicate that f₆/U₂ stage occurred prior to the emplacement of the Mackenzie diabase dykes at 1267 ± 2 Ma (LeCheminant and Heaman 1989) as well as the f₅/U₁ event. These observations bracket the f₆ stage between 1500 and 1267 Ma. Note however that no available absolute age dating supports this timing. The dated U₂ samples display ages at 565 ± 38 Ma and 345 ± 19 Ma at Andrew Lake. Shabaga et al. (2017) obtained ages at ca. 1000 Ma and 550–300 Ma. One likely explanation is related to alteration and reset/reprecipitation of U oxides that accounts for the modified REE bell-shaped pattern for U₂ oxides (Fig. 6a).

Like U₁, U₂ formed in relation to the circulations of basal brines derived from the Thelon Basin, and is of unconformity-related type. The differences (fracture orientations, intensity of clay alteration, reduced vs. oxidized fault zones, polymetallic vs. monometallic character) between mineralization events U₁ and U₂ are here interpreted as the distinctive response of pre-existing reactivated faults to a change in the regional tectonic stress field. This reactivation induced maturation of fault zones and likely a change in fluids pathway, hence contrasting fluid-rock interactions. U₁ and U₂ mineralization probably occurred between 1530 and 1267 Ma, an interval previously proposed for the crystallization of hydrothermal UO₂ in the area (Sharpe et al. 2015; Chi et al. 2017). URU-type mineralization in the Kiggavik area present two main differences with the Athabasca Basin are noted; the absence of dravite and Mg-foitite (Mg-tourmaline, Mercadier et al. 2012) and the presence of a Mg-rich sudoite rather than a Al-Mg sudoite.

(f₇) The last, post-ore main fracturing event is characterized by fault zones displaying strongly desilicified, illitized, and bleached fault rocks with numerous narrow fault cores. This event is temporally dissociated of U mineralization and reworks/offsets previously formed prospects along E-W and NW-SE faults (Fig. 15a). This stage had a significant impact on the 3D architecture of some prospects (e.g., Bong, End) because the related faults offset U orebodies with a significant dip-slip and a minor strike-slip component. This is especially obvious at Bong where the orebody is offset by W-E to WNW-ESE trending, nearly dip-slip normal faults, but also at End where the orebody is offset by NW-SE to NNW-SSE trending faults. Moreover, observed U₁- and U₂-bearing fault zones are also less mineralized when they are cross-cut by white clay-altered faults, indicating remobilization of the U oxides at this stage. Only trace relicts of pitchblende were observed in f₇ fault zones (Fig. 4j). As this event corresponds to one of the latest fracturing stages in a complex and poly-phase fault system, fracture orientations of this stage represent more reactivation than neoformation. Thus, it is difficult to process oriented data in order to retrieve the “true” fault

orientations. A WNW-ESE to NNW-SSE trend and a steep dip to the northwest however appear to be the dominant orientation of these faults in the Kiggavik area. Reactivation of faults during this stage is illustrated by NE-SW white clay-altered faults at Contact, initially belonging to the f6 stage (Grare et al. 2018a). This observation that most of the faults related to this post-ore fracturing stage are inherited is consistent with models in which reactivation of faults is often easier compared to neoformation (e.g., Pinheiro and Holdsworth 1997). f7 faults with kinematic data display two main trends: WNW-ESE with dextral to dextral-normal slip component and NNW-SSE with sinistral slip component. Combined with the dominant dip-slip component observed on some WNW-ESE faults observed at Bong, we infer a transtensional stress regime with σ_1 trending NW-SE and σ_3 trending NE-SW. This faulting event would be responsible for the down-drop offset of the U orebodies observed at Bong, End, and Kiggavik Main Zones (example in Fig. 4e). The NW-SE trending σ_1 and NE-SW trending σ_3 would also account for the latest sinistral offset of the Judge Sissons Fault and Thelon Fault by NNW-SSE faults, observed in the field and on aeromagnetic maps (Tschirhart et al. 2017). Such NNW-SSE faults were likely reopened during the emplacement of the Mackenzie dykes. The inferred NW-SE trending σ_1 and NE-SW trending σ_3 (Fig. 15b) are consistent with a regional compressional stress active on the southeast margin of the Canadian Shield (Hou et al. 2010) at ca. 1270 Ma. It is inferred that the emplacement of a mantle plume triggered the emplacement of Mackenzie mafic dykes swarm at that time. This magmatic event is likely at the origin of the circulation of hot (~ 300 °C), probably acidic, fluids during the f7 fracturing stage. This is supported by age dating on illite (K-Ar and Ar-Ar) from f7 fractures showing an alteration event at ca. 1300 Ma (Fig. 10) at End, Andrew Lake, Bong, and Kiggavik Main Zone. This tectonic/magmatic event ended by the emplacement of the MacKenzie diabase dykes which cross-cut orebodies and fault rocks. Along these dykes, hot fluids would have caused local remobilization and reprecipitation of U oxides, hence resetting of the U/Pb isotopic system. Such strong clay alteration has previously been described as synchronous with U alteration (Hasegawa et al. 1990; Riegler et al. 2014; Shabaga et al. 2017), but this study unambiguously shows that white clay illitization postdates U0, U1, and U2.

Post Mackenzie dykes minor fracturing events and U mineralization/remobilization (U3)

Several ages at ca. 1000 Ma and ca. 800 Ma were previously obtained from U oxides in the Kiggavik area (Fig. 10). These ages, not reproduced in the present study, could reflect a far-field tectonic activity associated with the Grenville orogeny (Gordon and Hempton 1986) and the initial rifting event of Rodinia (Badger et al. 2010; McClellan and Gazel 2014). It is

currently unclear whether these two events have led to the formation of new mineralization or simply caused alteration and reset of existing mineralization. Younger ages at ca. 550 Ma and ca. 350 Ma correspond to a reset of the U-Pb isotopic systems of U1 and U2 but also to their dissolution linked to circulation of meteoric fluids and precipitation of U3. The specific modified bell-shaped pattern marks the alteration and remobilization of the URU-type U oxides by low-T meteoric fluids, which is consistent with the observation of goethite in these mineralized samples. U3 occurred at a post-Mackenzie stage and does not belong to the unconformity-related type. It likely happened when a significant thickness of the Thelon Basin, Wharton Basin, and/or basement rocks was definitely eroded, letting supergene, low-temperature oxidizing fluids circulating through the fracture network and remobilizing U. Such (weak) reactivation of the fracture network is probably linked to a far-field stress associated with the breakup of West Rodinia supercontinent (ca. 500 Ma, Bond et al. 1984) and the Appalachian Orogeny (ca. 350 Ma, Hatcher, 2002). This event has also been recognized in the Athabasca Basin (Dieng et al. 2013).

The structural evolution proposed in this study differs from the model of Riedel shear system of Anand and Jefferson (2017). These authors proposed that the entire fracture network evolved mainly under a $\sim N110-N140^\circ$ trending σ_1 from ca. 1800 Ma to 1540 Ma. In their model, the different fault zones (oriented ENE-WSW, NNW-SSE, NS, NE-SW, E-W) are part of a single Riedel system (i.e., analogue to the P, T, X, R', R shears). Our structural analysis, together with the compilation of isotopic U-Pb ages and trace element concentrations for the different mineralization observed in the Kiggavik area, indicates that the U system was instead polyphase and that U was mobilized at several times during more than 1.5 billion years. Such extremely long duration of U events is similar to what has been observed in the Athabasca Basin. Additionally, the similarities between the Athabasca and Thelon Basins demonstrate that they had rather close evolution through time in terms of U systems, moving from relatively high-T magmatic conditions (U0) before 1750 Ma, to moderate-T hydrothermal conditions with basinal brines (U1 and U2) between 1530 to 1270 Ma to low-T meteoric mineralization (U3) later.

Conclusions

This paper proposes an integrated structural and metallogenic model of the Kiggavik area based on a multi-scale and multi-disciplinary approach. The main conclusions of the study are as follows:

- The Kiggavik area is characterized by a polyphase fault/fracture network that evolved in a brittle style from ca.

- 1830 Ma to the emplacement of the Mackenzie dykes at ca. 1270 Ma. The pre-Thelon Basin U0 mineralization and the Quartz Breccia event highlight the importance of magmatic-related fracturing, fluid circulation, and mineralization on controlling subsequent occurrence of URU prospects. U0 constituted a significant stock of U available for reconcentration through later circulation of oxidized basinal brines. This first mineralization is of magmatic-related type.
- After deposition of Thelon and Lookout Point formations, and before the MacKenzie dyke event, i.e., between 1530 and 1270 Ma, a first circulation of highly saline basinal brines derived from the Thelon Basin in basement structures occurred under a strike-slip stress regime with WNW-ESE σ_1 and NNE-SSW σ_3 . This event was associated with precipitation of U1 in fault relay zones and/or in fault zones where the Quartz Breccia was present. Faulting/fracturing and renewed circulations of basinal brines occurred under a stress regime with NE-SW σ_1 and NW-SE σ_3 which caused transpressional reactivation of the previously formed fault/fracture network and the formation of U2. U mineralization preferentially developed in moderately altered damage zones of faults. U1 and U2 mineralization belong to the unconformity-related (URU) type. They formed in relative similar conditions and timing than URU-type mineralization in the Athabasca Basin.
 - Circulation of basinal brines occurred through a fault/fracture network that evolved through time in response to the changing local/far-field tectonic stress. This caused changes in the fluid pathways hence in fluid-rock interaction (changing characteristics of the fluid such as fO_2 and pH) and led to slightly different U mineralization (polymetallic reduced U1 vs monometallic oxidized U2).
 - The initial NaCl-rich basinal brines reacted with basement rocks to form $CaCl_2$ - and metal-rich mineralizing brines at the origin of U1 and U2. The chemistry and physico-chemical characteristics of the $CaCl_2$ -rich brines in the Kiggavik area are similar to those measured for mineralizing $CaCl_2$ -rich brines in the Athabasca Basin, indicating rather common processes for the two sedimentary basins and related U mineralization.
 - Late faulting and associated strong clay alteration and bleaching of the host rock occurred at ca. 1300 Ma in response to local NE-SW extension. This fracturing event, barren of U mineralization, caused the offset of previously formed orebodies and accounts for the formation in the Kiggavik area of strongly altered areas disconnected of any U mineralization.
 - Weak reactivation of the fracture network after emplacement of the MacKenzie dykes induced circulation of low-T meteoric water, remobilizing and reprecipitating U oxides (U3) at two different times, ca. 550 and 350 Ma.

Other fluid circulation events likely happened at ca. 1000 and 700 Ma with similar processes.

- U mineralization in the Kiggavik area are of a mixed type, combining magmatic (U0), URU type (U1 and U2), and meteoric-related (“roll-front,” U3) mineralization, as proposed by previous studies in the Athabasca Basin. This area documents more than 1.5 billion years of U mobility.

Acknowledgments We thank Orano for the permission to publish these results. Special thanks to Dr. Kathryn Bethune for her in-depth review; senior petrographist M. Brouand; senior geoscientist D. Quirt; and ARC geologists R. Zerff, R. Hutchinson, K. Martin, and D. Hrabok for their help and enriching discussions during field work and data interpretation. Thanks to P. Martz for his help on studying fluid inclusions. We are grateful to N. Bouden, J. Villeneuve, and E. Deloule at CRPG (Vandoeuvre-lès-Nancy) for SIMS analyses, and to A. Lecomte and O. Rouer at SCMEM (GeoRessources, Vandoeuvre-lès-Nancy) for data acquisition. Thanks to J.M. Vergeau and P-C. Guiollard at Bessines-sur-Gartempe Areva site for the help and access to historical data and samples. The detailed reviews by Guoxiang Chi and an anonymous reviewer, and editorial suggestions by Associate Editor Mostafa Fayek and Editor-in-Chief Georges Beaudoin, have greatly improved the quality of this paper.

Funding information The authors thank Orano and Orano Canada for the full financial support and access to the Kiggavik camp and exploration data.

References

- Alexandre P, Kyser K, Thomas D et al (2009) Geochronology of unconformity-related uranium deposits in the Athabasca Basin, Saskatchewan, Canada and their integration in the evolution of the basin. *Miner Deposit* 44:41–59. <https://doi.org/10.1007/s00126-007-0153-3>
- Alexandre P, Kyser K, Layton-Matthews D et al (2015) Chemical compositions of natural uraninite. *Can Mineral* 53:595–622. <https://doi.org/10.3749/canmin.1500017>
- Allan MM, Yardley BW, Forbes LJ et al (2005) Validation of LA-ICP-MS fluid inclusion analysis with synthetic fluid inclusions. *Am Mineral* 90:1767–1775
- Anand A, Jefferson CW (2017) Reactivated fault systems and their effects on outcrop patterns of thin-skinned early thrust imbrications in the Kiggavik uranium camp, Nunavut. *Geol. Surv. Can.* 2017. Open File 7895. <https://doi.org/10.4095/302776>
- Ashcroft GS, Fayek M, Quirt D et al (2017) The geochemistry and geochronology of the end deposit, NE Thelon region. An insight to the Athabasca basin’s closest relative, Nunavut Canada, p 1
- Badger RL, Ashley KT, Cousens BL (2010) Stratigraphy and geochemistry of the Catocin volcanics: Implications for mantle evolution during the breakup of Rodinia. In: Tollo RP, Bartholomew MJ, Hibbard JP, Karabinos PM (eds) *From Rodinia to Pangea: The Lithotectonic Record of the Appalachian Region*. Geological Society of America. [https://doi.org/10.1130/2010.1206\(17\)](https://doi.org/10.1130/2010.1206(17))
- Battaglia S (2004) Variations in the chemical composition of illite from five geothermal fields: a possible geothermometer. *Clay Miner* 39: 501–510. <https://doi.org/10.1180/0009855043940150>
- Baudemont D, Reilly B (1997) Thelon Project - 1997: Reconnaissance Mapping and Structural Geology. Cogema internal report. 97-CND-100-01. 43p.

- Benedicto A, Schultz RA (2010) Stylolites in limestone: magnitude of contractional strain accommodated and scaling relationships. *J Struct Geol* 32:1250–1256. <https://doi.org/10.1016/j.jsg.2009.04.020>
- Blake DH (1980) Volcanic rocks of the Paleohelikian Dubawnt Group in the Baker Lake - Angikuni Lake area, district of Keewatin, N.W.T. Geological Survey of Canada, bulletin 309, 39p.
- Bond GC, Nickeson PA, Kominz MA (1984) Breakup of a supercontinent between 625 Ma and 555 Ma: new evidence and implications for continental histories. *Earth Planet Sci Lett* 70:325–345. [https://doi.org/10.1016/0012-821X\(84\)90017-7](https://doi.org/10.1016/0012-821X(84)90017-7)
- Bonhoure J, Kister P, Cuney M, Deloule E (2007) Methodology for rare earth element determinations of uranium oxides by ion microprobe. *Geostand Geoanal Res* 31:209–225. <https://doi.org/10.1111/j.1751-908X.2007.00865.x>
- Bourdelle F, Cathelineau M (2015) Low-temperature chlorite geothermometry: a graphical representation based on a T?R2? ?Si diagram. *Eur J Mineral* 27:617–626. <https://doi.org/10.1127/ejm/2015/0027-2467>
- van Breemen O, Peterson TD, Sandeman HA (2005) U–Pb zircon geochronology and Nd isotope geochemistry of Proterozoic granitoids in the western Churchill Province: intrusive age pattern and Archean source domains. *Can J Earth Sci* 42:339–377. <https://doi.org/10.1139/e05-007>
- Bridge J, Banerjee N, Pehrsson S et al (2013) Lac Cinquante uranium deposit, Western Churchill Province, Nunavut, Canada. *Explor Min Geol* 21:27–50
- Burma BH, Riley CM (1955) Two unusual occurrences of microstylolite. *J Sediment Res* 25:38–40. <https://doi.org/10.1306/D42697EC-2B26-11D7-8648000102C1865D>
- Caine JS, Evans JP, Forster CB (1996) Fault zone architecture and permeability structure. *Geology* 24:1025–1028
- Cathelineau M (1988) Cation site occupancy in chlorites and illites as a function of temperature. *Clay Miner* 23:471–485
- Cathelineau M, Boiron MC, Holliger P, Poty B (1990) Metallogenesis of the French part of the Variscan orogen. Part II: time-space relationships between U, Au and SnW ore deposition and geodynamic events — mineralogical and UPb data. *Tectonophysics* 177:59–79. [https://doi.org/10.1016/0040-1951\(90\)90274-C](https://doi.org/10.1016/0040-1951(90)90274-C)
- Chamberlain KR, Schmitt AK, Swapp SM et al (2010) In situ U–Pb SIMS (IN-SIMS) micro-baddeleyite dating of mafic rocks: method with examples. *Precambrian Res* 183:379–387. <https://doi.org/10.1016/j.precamres.2010.05.004>
- Chester FM, Logan JM (1986) Implications for mechanical properties of brittle faults from observations of the Punchbowl fault zone, California. *Pure Appl Geophys* 124:79–106. <https://doi.org/10.1007/BF00875720>
- Chi G, Haid T, Quirt D, Fayek M, Blamey N, Chu H (2017) Petrography, fluid inclusion analysis, and geochronology of the end uranium deposit, Kiggavik, Nunavut, Canada. *Mineral Deposita* 52:211–232. <https://doi.org/10.1007/s00126-016-0657-9>
- Chi G, Li Z, Chu H et al (2018) A shallow-burial mineralization model for the unconformity-related uranium deposits in the Athabasca Basin. *Econ Geol* 113:1209. <https://doi.org/10.5382/econgeo.2018.4588>
- Chu H, Chi G (2016) Thermal profiles inferred from fluid inclusion and illite geothermometry from sandstones of the Athabasca basin: implications for fluid flow and unconformity-related uranium mineralization. *Ore Geol Rev* 75:284–303. <https://doi.org/10.1016/j.oregeorev.2015.12.013>
- Cook FA (1992) Racklan Orogen. *Can J Earth Sci* 29:2490–2496. <https://doi.org/10.1139/e92-195>
- Cook DG, MacLean BC (1995) The intracratonic Paleoproterozoic forward orogeny, and implications for regional correlations, Northwest Territories, Canada. *Can J Earth Sci* 32:1991–2008. <https://doi.org/10.1139/e95-152>
- Corrigan D, Pehrsson S, Wodicka N, de Kemp E (2009) The Palaeoproterozoic Trans-Hudson Orogen: a prototype of modern accretionary processes. *Geol Soc Lond Spec Publ* 327:457–479. <https://doi.org/10.1144/SP327.19>
- Creaser RA, Stasiuk LD (2007) Depositional age of the Douglas formation, Northern Saskatchewan, determined by RE-Os geochronology. In: Jefferson C W, Delaney G, eds. EXTECH IV: Geology and Uranium EXploration TECHnology of the Proterozoic Athabasca Basin, Saskatchewan and Alberta; Geological Survey of Canada, Bulletin no. 588, 2007 p. 341–346; <https://doi.org/10.4095/223779>
- Cumming GL, Krstic D (1992) The age of unconformity-related uranium mineralization in the Athabasca Basin, northern Saskatchewan. *Can J Earth Sci* 29:1623–1639. <https://doi.org/10.1139/e92-128>
- Cuney M (2014) Felsic magmatism and uranium deposits. *Bull Soc Geol Fr* 185:75–92
- Cuney M, Kyser K (2009) Recent and not-so-recent developments in uranium deposits and implications for exploration. *Econ Geol* 104:600–601
- Cuney M, Kyser K (2015) The geology and geochemistry of uranium and thorium deposits. Mineralogical Association of Canada, Short Course Series Volume 46, Montreal, Quebec, 2015. Robert Raeside, Series Editor, 345 p. ISBN 978-0-0921294-57-3
- Curtis L, Miller AR (1980) Uranium geology in the Amer-Dubawnt-Yathkyed-Baker Lakes region, Keewatin district, NWT Canada. In: Ferguson J. and Goleby A. B. eds. Uranium in the Pine Creek geosyncline. Vienna: IAEA, 1980, 595–616
- Davis WJ, Hanmer S, Tella S et al (2006) U–Pb geochronology of the MacQuoid supracrustal belt and Cross Bay plutonic complex: Key components of the northwestern Hearne subdomain, western Churchill Province, Nunavut, Canada. *Precambrian Res* 145:53–80. <https://doi.org/10.1016/j.precamres.2005.11.016>
- Davis WJ, Gall Q, Jefferson CW, Rainbird RH (2011) Fluorapatite in the Paleoproterozoic Thelon Basin: structural-stratigraphic context, in situ ion microprobe U–Pb ages, and fluid-flow history. *GSA Bull* 123:1056–1073
- Depin  M, Frimmel HE, Emsbo P, Koenig AE, Kern M (2013) Trace element distribution in uraninite from Mesoarchaean Witwatersrand conglomerates (South Africa) supports placer model and magmatogenic source. *Mineral Deposita* 48:423–435. <https://doi.org/10.1007/s00126-013-0458-3>
- Derome D, Cathelineau M, Cuney M et al (2005) Mixing of Sodic and calcic brines and uranium deposition at McArthur River, Saskatchewan, Canada: a Raman and laser-induced breakdown spectroscopic study of fluid inclusions. *Econ Geol* 100:1529–1545. <https://doi.org/10.2113/gsecongeo.100.8.1529>
- Dieng S, Kyser K, Godin L (2013) Tectonic history of the North American shield recorded in uranium deposits in the Beaverlodge area, northern Saskatchewan, Canada. *Precambrian Res* 224:316–340. <https://doi.org/10.1016/j.precamres.2012.09.011>
- Dieng S, Kyser K, Godin L (2015) Genesis of multifarious uranium mineralization in the Beaverlodge area, northern Saskatchewan, Canada. *Econ Geol* 110:209–240
- Bloss FD (1954) Microstylolites in a rhyolite porphyry. *J Sediment Petrol* 24:252–254. doi: <https://doi.org/10.1306/D42697BA-2B26-11D7-8648000102C1865D>
- Dubacq B, Vidal O, De Andrade V (2010) Dehydration of dioctahedral aluminous phyllosilicates: thermodynamic modelling and implications for thermobarometric estimates. *Contrib Mineral Petrol* 159:159–174
- Dubessy J, Pagel M, Beny J, et al (1988) Radiolysis evidenced by Hz-O2 and Hz-bearing fluid inclusions in three uranium deposits. *Geochim Cosmochim Acta* 52:1155–1167. doi: [https://doi.org/10.1016/0016-7037\(88\)90269-4](https://doi.org/10.1016/0016-7037(88)90269-4)
- Dubessy J, Poty B, Ramboz C (1989) Advances in C–O–H–N–S fluid geochemistry based on micro-Raman spectrometric analysis of fluid

- inclusions. *Eur J Mineral* 1:517–534. <https://doi.org/10.1127/ejm/1/4/0517>
- Eglinger A, André-Mayer A-S, Vanderhaeghe O et al (2013) Geochemical signatures of uranium oxides in the Lufilian belt: from unconformity-related to syn-metamorphic uranium deposits during the Pan-African orogenic cycle. *Ore Geol Rev* 54:197–213. <https://doi.org/10.1016/j.oregeorev.2013.04.003>
- Ernst RE, Head JW, Parfitt E et al (1995) Giant radiating dyke swarms on Earth and Venus. *Earth Sci Rev* 39:1–58. [https://doi.org/10.1016/0012-8252\(95\)00017-5](https://doi.org/10.1016/0012-8252(95)00017-5)
- Farkas A (1984) Mineralogy and host rock alteration of the Lone Gull deposit. Urangesellschaft Internal Report, 44 pp.
- Faulkner DR, Jackson CAL, Lunn RJ et al (2010) A review of recent developments concerning the structure, mechanics and fluid flow properties of fault zones. *J Struct Geol* 32:1557–1575. <https://doi.org/10.1016/j.jsg.2010.06.009>
- Fayek M, Kyser TK, Riciputi LR (2002) U and Pb isotope analysis of uranium minerals by ion microprobe and the geochronology of McArthur River and Sue Zone Uranium deposits, Saskatchewan, Canada. *Can Mineral* 40:1553. <https://doi.org/10.2113/gscanmin.40.6.1553>
- Fayek M, Quirt D, Jefferson C, et al (2017) The Kiggavik-Andrew Lake structural trend uranium deposits: an overview. In: SGA Extended Abstract proceedings. SGA 2017 Conference Quebec City, August. pp 20–23
- Fossen H, Rotevatn A (2016) Fault linkage and relay structures in extensional settings—a review. *Earth Sci Rev* 154:14–28. <https://doi.org/10.1016/j.earscirev.2015.11.014>
- Friedrich G, Weyer HJ, Bectel A, Ballhorn RK (1989) The Lone Gull uranium deposit - new geochemical and petrological data as evidence for the nature of the ore bearing solutions. IAEA, Tech Comm Metallog uranium Depos:293–305
- Frimmel HE, Schedel S, Brätz H (2014) Uraninite chemistry as forensic tool for provenance analysis. *Appl Geochem* 48:104–121. <https://doi.org/10.1016/j.apgeochem.2014.07.013>
- Fuchs HD, Hilger W (1989) Kiggavik (lone gull): An unconformity related uranium deposit in the Thelon basin, Northwest Territories, Canada. In International Atomic Energy Agency Technical Committee Meeting, Saskatoon, Canada, 1–3 September 1987, IAEA TECDOC-500: 429–454
- Fuchs HD, Hilger W, Prosser E (1986) Geology and exploration history of the Lone Gull property. Canadian Institute of Mining and Metallurgy Special,33: 286–292
- Gall Q, Peterson TD, Donaldson J (1992) A proposed revision of Early Proterozoic stratigraphy of the Thelon and Baker Lake basins, Northwest Territories. *Geol Surv Canada Curr Res* 92–1c:129–137
- Golding HG, Conolly JR (1962) Stylolites in volcanic rocks. *J Sediment Res* 32:534–538. <https://doi.org/10.1306/74D70D12-2B21-11D7-8648000102C1865D>
- Gordon MB, Hempton MR (1986) Collision-induced rifting: the Grenville orogeny and the Keweenaw rift of North America. *Tectonophysics* 127:1–25. [https://doi.org/10.1016/0040-1951\(86\)90076-4](https://doi.org/10.1016/0040-1951(86)90076-4)
- Grare A, Benedicto A, Lacombe O, et al (2017) Structural controls on uranium mineralization at the Kiggavik project (NE Thelon area, Canada). In: Mineral Resources to Discover - 14th SGA Biennial Meeting in Quebec City, Canada. Volume 2 August 20-23. pp 739–742
- Grare A, Benedicto A, Lacombe O et al (2018a) The Contact uranium prospect, Kiggavik project, Nunavut (Canada): Tectonic history, structural constraints and timing of mineralization. *Ore Geol Rev* 93:141–167. <https://doi.org/10.1016/j.oregeorev.2017.12.015>
- Grare A, Lacombe O, Mercadier J et al (2018b) Fault zone evolution and development of a structural and hydrological barrier: the quartz breccia in the Kiggavik area (Nunavut, Canada) and its control on uranium mineralization. *Minerals* 8:319. <https://doi.org/10.3390/min8080319>
- Gueguen Y, Palciauskas V, Jeanloz R (1995) Introduction to physics of rocks. *Physics Today* 48, 4, 87 (1995); 294pp. <https://doi.org/10.1063/1.2807985>
- Hadlari T, Rainbird RH (2011) Retro-arc extension and continental rifting: a model for the Paleoproterozoic Baker Lake Basin, Nunavut. Geological Survey of Canada Contribution 20100436. *Can J Earth Sci* 48:1232–1258. <https://doi.org/10.1139/e11-002>
- Hasegawa K, Davidson GI, Wollenberg P, Lida Y (1990) Geophysical exploration for unconformity-related uranium deposits in the north-eastern part of the Thelon basin, northwest territories, Canada. *Kozan Chishitsu* 40:83–94
- Hecht L, Cuney M (2000) Hydrothermal alteration of monazite in the Precambrian crystalline basement of the Athabasca Basin (Saskatchewan, Canada): implications for the formation of unconformity-related uranium deposits. *Miner Depos* 35:791–795
- Hiatt EE, Kyser K, Dalrymple RW (2003) Relationships among sedimentology, stratigraphy, and diagenesis in the Proterozoic Thelon Basin, Nunavut, Canada: implications for paleo-aquifers and sedimentary-hosted mineral deposits. *J Geochem Explor* 80:221–240. [https://doi.org/10.1016/S0375-6742\(03\)00192-4](https://doi.org/10.1016/S0375-6742(03)00192-4)
- Hoeve J, Quirt DH (1984) Mineralization and host rock alteration in relation to clay mineral diagenesis and evolution of the middle-Proterozoic. Athabasca Basin, Northern Saskatchewan, Canada
- Hoffman PF (1988) United plates of America, the birth of a Craton: Early Proterozoic assembly and growth of Laurentia. *Annu Rev Earth Planet Sci* 16:543–603. <https://doi.org/10.1146/annurev.ea.16.050188.002551>
- Hou G, Kusky TM, Wang C, Wang Y (2010) Mechanics of the giant radiating Mackenzie dyke swarm: a paleostress field modeling. *J Geophys Res Solid Earth* 115:n/a-n/a. <https://doi.org/10.1029/2007JB005475>
- Hunt PA, Roddick JC (1988) A compilation of K-Ar ages: report 18. In: Radiogenic Age and Isotopic Studies: Report 2, Paper 88–2. Geological Survey of Canada, pp 127–153
- Hunt PA, Roddick JC (1992a) A compilation of K-Ar ages: report 21. In: Radiogenic Age and Isotopic Studies: Report 5, Paper 91–2. Geological Survey of Canada, pp 207–261
- Hunt PA, Roddick JC (1992b) A compilation of K-Ar and 40Ar-39Ar ages: report 22. In: Radiogenic Age and Isotopic Studies: Report 6, Paper 92–2. Geological Survey of Canada, pp 179–226
- Jeanneret P, Goncalves P, Durand C et al (2017) Geochronological constraints on the trans-Hudsonian tectono-metamorphic evolution of the pre-Athabasca basement within the Wollaston-Mudjatik Transition Zone, Saskatchewan. *Precambrian Res* 301:152–178. <https://doi.org/10.1016/j.precamres.2017.07.019>
- Jefferson CW, Thomas DJ, Gandhi S et al (2007) Unconformity-associated uranium deposits of the Athabasca Basin, Saskatchewan and Alberta. In: Jefferson C W, Delaney G, eds. EXTECH IV: Geology and Uranium Exploration TECHNOLOGY of the Proterozoic Athabasca Basin, Saskatchewan and Alberta. Geological Survey of Canada, Bulletin no. 588, 2007 p. 23–67
- Jefferson C, Pehrsson S, Peterson T, et al (2011) Northeast Thelon region geoscience framework - new maps and data for uranium in Nunavut. Geological Survey of Canada Open File 6950. doi: <https://doi.org/10.4095/288791>
- Johnstone D, Bethune K, Quirt D, Benedicto A (2016) Lithostratigraphic and structural controls of uranium mineralization in the Kiggavik East, Centre, and Main Zone Deposits, Thelon Basin: a potential analogue for the Athabasca Basin. In: Saskatchewan geological survey (ed) Saskatchewan Open House. Saskatoon, p 47
- Johnstone D, Bethune K, Quirt D, et al (2017) Lithostratigraphic and structural controls of uranium mineralization in the Kiggavik East Zone, Centre Zone, and Main Zone deposits, north-central Rae Subprovince, Nunavut, Canada. In: P. M-L (ed) 14th Biennial

- SGA Meeting: Mineral Resources to Discover, Vol. 2. Québec, pp 393–817
- Jowett EC (1991) Fitting iron and magnesium into the hydrothermal chlorite geothermometer. In: GAC/MAC/SEG Joint Annual Meeting, Toronto, May 27–29, 1991, Program with Abstracts 16
- Kim Y-S, Peacock DCP, Sanderson DJ (2004) Fault damage zones. *J Struct Geol* 26:503–517. <https://doi.org/10.1016/j.jsg.2003.08.002>
- Kotzer TG, Kyser TK (1995) Petrogenesis of the Proterozoic Athabasca Basin, northern Saskatchewan, Canada, and its relation to diagenesis, hydrothermal uranium mineralization and paleohydrogeology. *Chem Geol* 120:45–89. [https://doi.org/10.1016/0009-2541\(94\)00114-N](https://doi.org/10.1016/0009-2541(94)00114-N)
- Kranidiotis P, MacLean WH (1987) Systematics of chlorite alteration at the Phelps dodge massive sulfide deposit, Matagami, Quebec. *Econ Geol* 82:1898–1911. <https://doi.org/10.2113/gsecongeo.82.7.1898>
- Lach P, Mercadier J, Dubessy J et al (2013) In situ quantitative measurement of rare earth elements in uranium oxides by laser ablation-inductively coupled plasma-mass spectrometry. *Geostand Geoanal Res* 37:277–296. <https://doi.org/10.1111/j.1751-908X.2012.00161.x>
- LeCheminant AN, Heaman LM (1989) Mackenzie igneous events, Canada: Middle Proterozoic hotspot magmatism associated with ocean opening. *Earth Planet Sci Lett* 96:38–48. [https://doi.org/10.1016/0012-821X\(89\)90122-2](https://doi.org/10.1016/0012-821X(89)90122-2)
- LeCheminant AN, Miller AR, Booth GW, et al (1979) Geological Studies: Tebesjuak Map Area, District of Keewatin, Current Research, Part A. Geological Survey of Canada, Paper 79-1A, pp. 179–186.
- LeCheminant AN, Miller AR, LeCheminant GM (1987) Early Proterozoic alkaline igneous rocks, district of Keewatin, Canada: petrogenesis and mineralization. *Geol Soc Lond Spec Publ* 33: 219–240. <https://doi.org/10.1144/GSL.SP.1987.033.01.16>
- Leisen M, Boiron M-C, Richard A, Dubessy J (2012) Determination of Cl and Br concentrations in individual fluid inclusions by combining microthermometry and LA-ICPMS analysis: Implications for the origin of salinity in crustal fluids. *Chem Geol* 330–331:197–206. <https://doi.org/10.1016/j.chemgeo.2012.09.003>
- Lespinnasse M (1999) Are fluid inclusion planes useful in structural geology? *J Struct Geol* 21:1237–1243. [https://doi.org/10.1016/S0191-8141\(99\)00027-9](https://doi.org/10.1016/S0191-8141(99)00027-9)
- Lespinnasse M, Pêcher A (1986) Microfracturing and regional stress field: a study of the preferred orientations of fluid-inclusion planes in a granite from the Massif Central, France. *J Struct Geol* 8:169–180. [https://doi.org/10.1016/0191-8141\(86\)90107-0](https://doi.org/10.1016/0191-8141(86)90107-0)
- Lespinnasse M, Désindes L, Fratzek P, Petrov V (2005) Microfissural mapping of natural cracks in rocks: implications for fluid transfers quantification in the crust. *Chem Geol* 223:170–178. <https://doi.org/10.1016/j.chemgeo.2005.05.009>
- Lida Y (1997) Geochemical and Mineralogical studies - 1997 Sissons Project Urangesellschaft Internal Report
- Ludwig K (2007) Isoplot/Ex version 3.41b, a geochronological toolkit for Microsoft Excel. Berkeley Geochronol Cent Spec Publ No 4
- Martz P, Cathelineau M, Mercadier J et al (2017) C-O-H-N fluids circulations and graphite precipitation in reactivated Hudsonian shear zones during basement uplift of the Wollaston-Mudjatik Transition Zone: example of the cigar Lake U deposit. *Lithos* 294–295:222–245. <https://doi.org/10.1016/j.lithos.2017.10.001>
- Martz P, Mercadier J, Cathelineau M et al (2018) Formation of U-rich mineralizing fluids through basinal brine migration within basement-hosted shear zones: a large-scale study of the fluid chemistry around the unconformity-related Cigar Lake U deposit (Saskatchewan, Canada). *Chem Geol*. <https://doi.org/10.1016/j.chemgeo.2018.05.042>
- McClellan E, Gazel E (2014) The Cryogenian intra-continental rifting of Rodinia: evidence from the Laurentian margin in eastern North America. *Lithos* 206–207:321–337. <https://doi.org/10.1016/j.lithos.2014.08.006>
- Mercadier J, Richard A, Boiron MC et al (2010) Migration of brines in the basement rocks of the Athabasca Basin through microfracture networks (P-Patch U deposit, Canada). *Lithos* 115:121–136. <https://doi.org/10.1016/j.lithos.2009.11.010>
- Mercadier J, Cuney M, Cathelineau M, Lacorde M (2011a) U redox fronts and kaolinisation in basement-hosted unconformity-related U ores of the Athabasca Basin (Canada): late U remobilisation by meteoric fluids. *Miner Deposita* 46:105–135. <https://doi.org/10.1007/s00126-010-0314-7>
- Mercadier J, Cuney M, Lach P et al (2011b) Origin of uranium deposits revealed by their rare earth element signature. *Terra Nova* 23:264–269. <https://doi.org/10.1111/j.1365-3121.2011.01008.x>
- Mercadier J, Richard A, Cathelineau M (2012) Boron- and magnesium-rich marine brines at the origin of giant unconformity-related uranium deposits: $\delta^{11}\text{B}$ evidence from Mg-tourmalines. *Geology* 40: 231. <https://doi.org/10.1130/G32509.1>
- Mercadier J, Annesley IR, McKechnie CL et al (2013) Magmatic and metamorphic Uraninite mineralization in the Western margin of the Trans-Hudson Orogen (Saskatchewan, Canada): a uranium source for unconformity-related uranium deposits? *Econ Geol* 108:1037. <https://doi.org/10.2113/econgeo.108.5.1037>
- Miller AR (1980) Uranium Geology of the eastern Baker Lake Basin, District of Keewatin, Northwest Territories: Geological Survey of Canada, Bulletin 330, 63 p.
- Miller AR (1982) Alteration and mineralization types: Amer-Thelon area, NTS 66G, H District of Keewatin, N.W.T. Pref to Res Doc #1 Westmin Resour Ltd
- Miller AR (1995) Polymetallic unconformity-related uranium veins in lower Proterozoic Amer Group, Pelly Lake map area, northern Thelon Basin, Churchill Province, Northwest territories. *Curr Res* 1995-C; *Geol Surv Canada* 151–161
- Miller AR (1997) Petrography and mineral chemistry of the Jane Prospect : a platinum group element-bearing basement-hosted unconformity-related uranium deposit type. Cogema Resources Inc. Internal Report, 128p.
- Miller AR, Blackwell GW (1992) Petrology of alkaline rare earth element - bearing plutonic rocks, Enekatka Lake [65e/15] and Carey Lake [65l/7] map - Areas, District of Mackenzie. *Geol Surv Canada, Open File* 2484:129–134. <https://doi.org/10.4095/133336>
- Miller AR, LeCheminant AN (1985) Geology and uranium metallogeny of Proterozoic supracrustal successions, central district of Keewatin 19
- Miller AR, Stanton RA, Cluff GR, Male MJ (1986) Uranium deposits and prospects of the Baker Lake Basin and subbasins, Central District of Keewatin, Northwest Territories. *Uranium Depos Canada, CIM Spec Vol* 33:23
- Ng R, Alexandre P, Kyser K (2013) Mineralogical and geochemical evolution of the unconformity-related McArthur River zone 4 Orebody in the Athabasca Basin, Canada: implications of a silicified zone*. *Econ Geol* 108:1657. <https://doi.org/10.2113/econgeo.108.7.1657>
- Pacquet A (1993a) Report 8493 Canada Kiggavik Main zone D.H. 306 (93-UGC-92-01) - petrography and XRD analysis. Cogema Resources Inc. Internal report, 19p.
- Pacquet A (1993b) Report 8494 - Canada - Sissons Schultz South - End Grid DH END 42 - Petrography and XRD analysis. Cogema Resources Inc. Internal report, 14p.
- Pacquet A (1993c) Report 8556 - XRD - Andrew Lake Centre (lower lens) DH SW 78. Cogema Resources Inc. Internal report, 2p.
- Pacquet A (1994) Report 8549 - Canada (NWT) Andrew Lake DH SW 73 - petrography and XRD. Cogema Resources Inc. Internal report, 12p.
- Pagel M (1975) Cadre géologique des gisements d'uranium dans la structure de Carswell (Saskatchewan, Canada). *Etudes des phases*

- fluides. Thèse de 3ème cycle, Université de Nancy, Nancy, France. 171
- Pascal M, Ansdell K, Annesley I (2015) Graphite-bearing and graphite-depleted basement rocks in the Dufferin Lake zone, south-central Athabasca Basin, Saskatchewan. In: Potter EG, Wright DM, eds. Targeted Geoscience Initiative 4: unconformity-related uranium systems. Open File 7791, 83–92
- Pascal M, Boiron M-C, Ansdell K, Annesley IR, Kotzer T, Jiricka D, Cuney M (2016) Fluids preserved in variably altered graphitic pelitic schists in the Dufferin Lake zone, south-central Athabasca Basin, Canada: implications for graphite loss and uranium deposition. *Mineral Deposita* 51:619–636. <https://doi.org/10.1007/s00126-015-0628-6>
- Pehrsson SJ, Berman RG, Eglinton B, Rainbird R (2013) Two Neoproterozoic supercontinents revisited: the case for a Rae family of cratons. *Precambrian Res* 232:27–43. <https://doi.org/10.1016/j.precamres.2013.02.005>
- Peterson TD (2006) Geology of the Dubawnt Lake area, Nunavut-Northwest Territories Bull Geol Surv Canada 580
- Peterson TD (2015) Geological setting and geochemistry of the ca. 2.6 Ga Snow island Suite in the central Rae Domain of the Western Churchill Province, Nunavut. Geol Surv Canada Open File 7841 no. 29
- Peterson TD, Van Breemen O, Sandeman H, Cousens B (2002) Proterozoic (1.85–1.75 Ga) igneous suites of the Western Churchill Province: granitoid and ultrapotassic magmatism in a reworked Archean hinterland. *Precambrian Res* 119:73–100. [https://doi.org/10.1016/S0301-9268\(02\)00118-3](https://doi.org/10.1016/S0301-9268(02)00118-3)
- Peterson TD, Scott JMJ, Jefferson CW (2011) Uranium-rich bostonite-carbonatite dykes in Nunavut: recent observations Geological Survey of Canada Current Research 2011-11. 12p.
- Peterson TD, Scott JMJ, LeCheminant AN et al (2015) The Kivalliq Igneous Suite: Anorogenic bimodal magmatism at 1.75Ga in the western Churchill Province, Canada. *Precambrian Res* 262:101–119. <https://doi.org/10.1016/j.precamres.2015.02.019>
- Pinheiro RVL, Holdsworth RE (1997) Reactivation of Archean strike-slip fault systems, Amazon region, Brazil. *J Geol Soc Lond* 154:99–103. <https://doi.org/10.1144/gsjgs.154.1.0099>
- Rainbird RH, Davis WJ (2007) U-Pb detrital zircon geochronology and provenance of the late Paleoproterozoic Dubawnt Supergroup: linking sedimentation with tectonic reworking of the western Churchill Province, Canada. *GSA Bull* 119:314. <https://doi.org/10.1130/B25989.1>
- Rainbird RH, Hadlari T, Aspler LB et al (2003) Sequence stratigraphy and evolution of the paleoproterozoic intracontinental Baker Lake and Thelon basins, western Churchill Province, Nunavut, Canada. *Precambrian Res* 125:21–53. [https://doi.org/10.1016/S0301-9268\(03\)00076-7](https://doi.org/10.1016/S0301-9268(03)00076-7)
- Rainbird RH, Davis WJ, Stern RA et al (2006) Ar-Ar and U-Pb geochronology of a Late Paleoproterozoic Rift Basin: support for a genetic link with Hudsonian Orogenesis, Western Churchill Province, Nunavut, Canada. *J Geol* 114:1–17. <https://doi.org/10.1086/498097>
- Rainbird RH, Davis WJ, Pehrsson SJ et al (2010) Early Paleoproterozoic supracrustal assemblages of the Rae domain, Nunavut, Canada: intracratonic basin development during supercontinent break-up and assembly. *Precambrian Res* 181:167–186. <https://doi.org/10.1016/j.precamres.2010.06.005>
- Renac C, Kyser TK, Durocher K et al (2002) Comparison of diagenetic fluids in the Proterozoic Thelon and Athabasca Basins, Canada: implications for protracted fluid histories in stable intracratonic basins. *Can J Earth Sci* 39:113–132. <https://doi.org/10.1139/e01-077>
- Richard A (2017) Radiolytic (H₂, O₂) and other trace gases (CO₂, CH₄, C₂H₆, N₂) in fluid inclusions from unconformity-related U deposits. *Procedia Earth Planet Sci* 17:273–276. <https://doi.org/10.1016/j.proeps.2016.12.053>
- Richard A, Pettke T, Cathelineau M, et al (2010) Brine – rock interaction in the Athabasca basement (McArthur River U deposit , Canada): consequences for fluid chemistry and uranium uptake. 303–308. doi: <https://doi.org/10.1111/j.1365-3121.2010.00947.x>
- Richard A, Banks DA, Mercadier J et al (2011) An evaporated seawater origin for the ore-forming brines in unconformity-related uranium deposits (Athabasca Basin, Canada): Cl/Br and $\delta^{37}\text{Cl}$ analysis of fluid inclusions. *Geochim Cosmochim Acta* 75:2792–2810. <https://doi.org/10.1016/j.gca.2011.02.026>
- Richard A, Cauzid J, Cathelineau M, et al (2012) Synchrotron XRF and XANES investigation of uranium speciation and element distribution in fluid inclusions from unconformity-related uranium deposits. *Geofluids* 13:101–111. doi: <https://doi.org/10.1111/gfl.12009>
- Richard A, Boulvais P, Mercadier J et al (2013) From evaporated seawater to uranium-mineralizing brines: isotopic and trace element study of quartz – dolomite veins in the Athabasca system. *Geochim Cosmochim Acta* 113:38–59. <https://doi.org/10.1016/j.gca.2013.03.009>
- Richard A, Kendrick MA, Cathelineau M (2014) Noble gases (Ar, Kr, Xe) and halogens (Cl, Br, I) in fluid inclusions from the Athabasca Basin (Canada): implications for unconformity-related U deposits. *Precambrian Res* 247:110–125. doi: <https://doi.org/10.1016/j.precamres.2014.03.020>
- Richard A, Montel J, Leborgne R, et al (2015) Monazite alteration in H₂O±HCl±NaCl ±CaCl₂ fluids at 150 °C and psat: implications for uranium deposits. 693–706. doi: <https://doi.org/10.3390/min5040518>
- Richard A, Cathelineau M, Boiron M-C et al (2016) Metal-rich fluid inclusions provide new insights into unconformity-related U deposits (Athabasca Basin and basement, Canada). *Mineral Deposita* 51:249–270
- Riegler T (2013) Système d'altération et minéralisation en uranium le long du faisceau structural Kiggavik - Andrew Lake (Nunavut, Canada) : modèle génétique et guides d'exploration. **Poitiers**
- Riegler T, Lescuyer J-L, Wollenberg P et al (2014) Alteration related to uranium deposits in the Kiggavik-Andrew Lake structural trend, Nunavut, Canada: new insights from clay mineralogy and petrography. *Can Mineral* 52:27–45. <https://doi.org/10.3749/canmin.52.1.27>
- Riegler T, Quirt D, Beaufort D (2016) Spatial distribution and compositional variation of APS minerals related to uranium deposits in the Kiggavik-Andrew Lake structural trend, Nunavut, Canada. *Mineral Deposita* 51:219–236. <https://doi.org/10.1007/s00126-015-0595-y>
- Rotevatn A, Bastesen E (2014) Fault linkage and damage zone architecture in tight carbonate rocks in the Suez Rift (Egypt): implications for permeability structure along segmented normal faults. *Geol Soc Lond Spec Publ* 374:79–95. <https://doi.org/10.1144/SP374.12>
- Roy R, Benedicto A, Grare A et al (2017) Three-dimensional gravity modelling applied to the exploration of uranium unconformity-related basement-hosted deposits: the Contact prospect case study, Kiggavik, northeast Thelon region (Nunavut, Canada). *Can J Earth Sci* 54:869–882. <https://doi.org/10.1139/cjes-2016-0225>
- Rutter EH (1983) Pressure solution in nature, theory and experiment. *J Geol Soc Lond* 140:725–740. <https://doi.org/10.1144/gsjgs.140.5.0725>
- Scott J, Peterson TD (2012) U, Th, and REE occurrences within Nueltin granite at Nueltin Lake, Nunavut: recent observations, *Geol Surv Canada. Curr Ther Res*: 2012-1, pp. 1–11
- Scott JMJ, Peterson TD, Jefferson CW, Cousens BL (2015) Petrology and geochronology of Paleoproterozoic intrusive rocks, Kiggavik uranium camp, Nunavut. *Can J Earth Sci* 518:1–80. <https://doi.org/10.1139/cjes-2014-0153>
- Shabaga BM, Fayek M, Quirt D et al (2017) Mineralogy, geochronology, and genesis of the Andrew Lake uranium deposit, Thelon Basin, Nunavut, Canada. *Can J Earth Sci* 54:850–868. <https://doi.org/10.1139/cjes-2017-0024>

- Sharpe R, Fayek M, Quirt D, Jefferson CW (2015) Geochronology and genesis of the bong uranium deposit, Thelon Basin, Nunavut, Canada. *Econ Geol* 110:1759–1777. <https://doi.org/10.2113/econgeo.110.7.1759>
- Stacey JS, Kramers JD (1975) Approximation of terrestrial lead isotope evolution by a two-stage model. *Earth Planet Sci Lett* 26:207–221. [https://doi.org/10.1016/0012-821X\(75\)90088-6](https://doi.org/10.1016/0012-821X(75)90088-6)
- Thorkelson D (2000) Geology and mineral occurrences of the Slats Creek, Fairchild Lake and “Dolores Creek” areas, Wernecke Mountains, Yukon Territory. Exploration and Geological Services Division, Yukon Region, Indian and Northern Affairs Canada, Bulletin 10, 73
- Tschirhart P, Morris WA, Jefferson CW (2013) Geophysical modeling of the Neoproterozoic Woodburn Lake and Paleoproterozoic Ketyet River groups, and plutonic rocks in central Schultz Lake map area, Nunavut. Geological Survey of Canada, Current Research 2013-2, p. 19
- Tschirhart V, Jefferson CW, Morris WA (2017) Basement geology beneath the northeast Thelon Basin, Nunavut: insights from integrating new gravity, magnetic and geological data. *Geophys Prospect* 65: 617–636. <https://doi.org/10.1111/1365-2478.12430>
- Turner W, Richards J, Nesbitt B, Muehlenbachs K, Biczok J (2001) Proterozoic low-sulfidation epithermal Au–Ag mineralization in the Mallery Lake area, Nunavut, Canada. *Mineral Deposita* 36: 442–457. <https://doi.org/10.1007/s001260100181>
- Turner WA, Heaman LM, Creaser RA (2003) Sm–Nd fluorite dating of Proterozoic low-sulfidation epithermal Au–Ag deposits and U–Pb zircon dating of host rocks at Mallery Lake, Nunavut, Canada. *Can J Earth Sci* 40:1789–1804. <https://doi.org/10.1139/e03-061>
- Velde B (ed) (1985) III-General Phase Diagrams for Some Clay Mineral Assemblages. In: *Clay Minerals*. Elsevier, pp 257–357. [https://doi.org/10.1016/S0070-4571\(08\)70114-6](https://doi.org/10.1016/S0070-4571(08)70114-6)
- Wang K, Chi G, Bethune KM, Card CD (2015) Fluid composition, thermal conditions, fluid-structural relationships and graphite alteration of the Phoenix Uranium Deposit, Athabasca Basin, Saskatchewan. In: Potter EG, Wright DM (eds) Targeted geoscience initiative 4: unconformity-related uranium systems, Open file. Natural Resources, Canada, p 126
- Wang K, Chi G, Bethune KM et al (2018) Fluid P-T-X characteristics and evidence for boiling in the formation of the Phoenix uranium deposit (Athabasca Basin, Canada): implications for unconformity-related uranium mineralization mechanisms. *Ore Geol Rev* 101:122–142. <https://doi.org/10.1016/j.oregeorev.2018.07.010>
- Weyer HJ, Friedrich G, Bechtel A, Ballhorn RK (1987) The Lone Gull Uranium deposit: new geochemical and petrological data as evidence for the nature of the ore bearing solutions. International Atomic Energy Agency Report TC542/19.
- Wibberley CAJ, Yielding G, Di Toro G (2008) Recent advances in the understanding of fault zone internal structure: a review. *Intern Struct Fault Zo Implic Mech Fluid-Flow Prop* 299:5–33. <https://doi.org/10.1144/SP299.2>
- Williams JH, Johnson CD (2004) Acoustic and optical borehole-wall imaging for fractured-rock aquifer studies. *J Appl Geophys* 55: 151–159. <https://doi.org/10.1016/j.jappgeo.2003.06.009>
- Zang W, Fyfe WS (1995) Chloritization of the hydrothermally altered bedrock at the Igarap{é} Bahia gold deposit, Caraj{á}s, Brazil. *Mineral Deposita* 30:30–38. <https://doi.org/10.1007/BF00208874>

Publisher's note Springer Nature remains neutral with regard to jurisdictional claims in published maps and institutional affiliations.